

Clustering of particles in turbulence due to phoresis

Lukas Schmidt¹, Itzhak Fouxon^{1,2}, Dominik Krug³, Maarten van Reeuwijk⁴, and Markus Holzner¹

¹ *ETH Zurich, Stefano Franscini-Platz 5, 8093 Zurich, Switzerland*

² *Department of Computational Science and Engineering, Yonsei University, Seoul 120-749, South Korea*

³ *Department of Mechanical Engineering, The University of Melbourne, Parkville, VIC 3010, Australia and*

⁴ *Department of Civil and Environmental Engineering, Imperial College London, London SW7 2AZ, UK*

We demonstrate that diffusiophoretic, thermophoretic and chemotactic phenomena in turbulence lead to clustering of particles on multi-fractal sets that can be described using one single framework, valid when the particle size is much smaller than the smallest length scale of turbulence l_0 . To quantify the clustering, we derive positive pair correlations and fractal dimensions that hold for scales smaller than l_0 . Statistics of the number of particles in a small volume are non-Poissonian manifesting deviations from the case of uncorrelated particles. For scales larger than l_0 we predict a stretched exponential decay to 1 of the pair correlation function. For the case of inhomogeneous turbulence we find that the fractal dimension depends on the inhomogeneous direction. By performing experiments of clustering of diffusiophoretic particles induced by salinity gradients in a turbulent gravity current we demonstrate clustering in conformity to the theory. The particle size in the experiment is comparable to l_0 , outside the strict validity region of the theory, suggesting that the theoretical predictions transfer to this practically relevant regime. This clustering mechanism can provide the key to the understanding of a multitude of processes such as formation of marine snow in the ocean and population dynamics of chemotactic bacteria.

PACS numbers: 47.10.Fg, 05.45.Df, 47.53.+n

I. INTRODUCTION

Inhomogeneous random distributions of advected fields like temperature, concentrations of salt or nutrients occur ubiquitously in fluids due to turbulence [1, 2]. For particles that perform phoresis (i.e. steady drift) in the gradients of the convected fields, the fields' inhomogeneities imply a finite velocity difference between the local flow and the particles [3]. Particles that perform thermophoresis in a fluid at rest (steady drift in constant temperature gradient) will drift through thermal convection flow and particles that perform diffusiophoresis (steady drift in constant gradient of salinity) will drift through the turbulent ocean. Thus while the turbulence is incompressible so that the steady-state distribution of tracers is uniform, the distribution of particles that perform phoresis can be inhomogeneous. In this work we demonstrate that this distribution occurs on a multifractal set with power-law pair correlations.

Preferential concentration is well-studied in the case of inertial particles [4–33] where it plays an important role in a wide range of phenomena including aerosols spreading in the atmosphere [34, 35], planetary physics [36], transport of materials by air or by liquids [37], liquid fuel combustion engines [38], rain formation in liquid clouds [6, 7, 19, 39] and many more. Inertia produces a small but finite difference between the particle's velocity and the local velocity of the fluid. This difference is determined uniquely by the local flow so the particles' motion in space is a smooth flow given by the local turbulent flow corrected by drift. Though the drift component is small it is compressible causing accumulation of particles with time in preferred regions of the flow and an inhomoge-

neous steady state distribution [4]. This parallels the ordinary centrifuge where uniform initial distributions of inertial and tracer particles become completely different with time. While inertial particles, however small their inertia is, will eventually accumulate on the boundary of the centrifuge, the tracer distribution will always stay uniformly distributed. In the case of turbulence the "boundary" on which inertial particles concentrate becomes very complex and time-dependent but it still has zero volume being multi-fractal [6, 8, 19].

The statistics of preferential particle concentration in turbulent flows obeying the incompressible Navier-Stokes equations can be described theoretically in a universal framework for weakly compressible flows [6, 19, 39], for particles much smaller than the Kolmogorov lengthscale. The complete statistics of concentration depend on the statistics of turbulence through one number only. This number provides the scaling exponent of the power-law correlations of the particle concentration. Thus different flows (large or smaller Reynolds number, including chaotic spatially uniform random flows) characterized by identical values of that number will have identical statistics of distribution of transported particles. This universality is the reason for recent observations of preferential concentration of living phytoplankton cells [40]. Though single cell motion is very different from the one of an inertial particle, both can be described with smooth spatial flow in a range of parameters. The flows are quite different but both are weakly compressible. Theory then implies identical statistics of inertial particles and phytoplankton which is confirmed experimentally. Thus the discussed phenomena become relevant in plankton population dynamics [41, 42].

There is indirect evidence that preferential concentration occurs for phoretic particles. Diffusiophoretic drift (due to salinity gradients) has been observed in microfluidic laminar flows [43], and has been shown to significantly affect the particles' distributions. Recent experimental and numerical investigations have provided additional insight in the effect of diffusiophoresis in chaotic flows [44, 45]. Numerical simulations have shown that chemotactic bacteria may accumulate in nutrient patches in a turbulent flow [46]. Thermophoresis leads to concentration in temperature minima or away from minima depending on their inertia [47]. However, clustering of any kind of phoretic particles in fully turbulent flows have neither been observed nor described theoretically.

In this paper we extend the universal framework for weakly compressible flow [19] to phoretic particles, leading to a prediction for the fractal dimension of the expected particle concentration in an inhomogeneous turbulent flow. The theory is validated experimentally using high-frequency 3-D velocity and density measurements of diffusiophoretic particles in a fully turbulent gravity current. The paper is structured as follows. In section II, a general introduction of phoretic particles and their governing equations is provided. The theory of clustering in homogeneous turbulence is described in section III, and is extended to inhomogeneous turbulence in section IV. Theoretical study of pair correlations outside the scale of smoothness is provided in section V. Fluctuations of the number of particles in a given volume are discussed in section VI. The results from laboratory experiments of a turbulent gravity current are discussed in section VII, and demonstrate phoretic clustering in agreement with the theory, despite having particle sizes comparable to the Batchelor scale which are formally outside of the validity region of the theory. Concluding remarks are made in section VIII, including the implications these findings may have on the formation of marine snow, which is the settling of organic particle aggregates in the ocean.

II. PHORESIS IN TURBULENT FLOWS

Phoresis is a universal phenomenon of steady drift of macroscopic particles in an inhomogeneous medium due to gradients in a scalar field $\phi(\mathbf{x})$. Gradients in ϕ cause a difference in forcing on different sides of a particle's surface, resulting in particle motion. The direction of movement depends on the underlying physics of the phoresis. In the isotropic case the motion is parallel to the gradient of the field so that the phoretic velocity \mathbf{v}_{ph} generally is

$$\mathbf{v}_{ph} = c_{ph} \nabla \phi, \quad (1)$$

where $c_{ph}(\mathbf{x}(t), \phi[\mathbf{x}(t)])$ is the phoretic coefficient that can depend on the particle position $\mathbf{x}(t)$ through the dependence on ϕ or other local fields (e.g density). It is assumed that the variation of $\phi(\mathbf{x})$ over the particle's size is small. If it is not then higher powers of $\nabla \phi$ and higher-order derivatives of ϕ contribute to \mathbf{v}_{ph} . The phoretic

velocity \mathbf{v}_{ph} is attained after transients that take finite relaxation time τ_{rel} during which the particle passes a characteristic distance $v_{ph}\tau_{rel}$.

The phoretic coefficient c_{ph} can be both positive or negative, and will depend on the type of phoresis, cf. Table I. In the case of thermophoresis the particle reacts to the gradient of temperature of the fluid T so that $\phi = T$. In gases the random hits of macroscopic particle from the gas molecules are stronger at the particles' side closer to higher temperature fluid. The particle is driven to regions with lower temperature so c_T in table I is negative. In liquids or in gases when small particles are considered the interactions are more complex and both signs of c_T can hold, see [48, 49] and references therein.

Diffusiophoresis is the drift of a colloidal particle in response to a gradient of the concentration C of a molecular solute [3, 50]. The drift velocity \mathbf{v}_d obeys $\mathbf{v}_d \approx D_p \nabla \ln C$. For electrolyte solutions (such as saltwater), which will be studied experimentally in section V, D_p is the diffusiophoretic constant that describes electrical and chemical couplings in the interfacial region between the particle surface and the surrounding solute inducing the drift [43, 50]. The diffusiophoretic constant depends on the particle's zeta (ζ)-potential (a measure for the electrokinetic surface potential) and the salt properties [50]. In the case of electrophoresis one can use Smoluchowski's [51] formula $c_E = \epsilon \zeta / (4\pi \eta_f)$ where ϵ is fluid permittivity and μ is the dynamic fluid viscosity. The behavior of c_{ph} depends on the phoresis: for diffusiophoresis in ionic solutions D_p can be considered constant but in the case of chemotaxis the chemical sensitivity χ can depend on the local concentration of the attractant [52, 53].

Infinite fluids are Galilean invariant so in the fluid that moves as a whole at constant speed \mathbf{u} the phoretic velocity becomes the sum of the fluid velocity \mathbf{u} plus the phoretic drift velocity,

$$\mathbf{v}_{ph}(t) = \mathbf{u} + c_{ph}[\mathbf{x}(t)] \nabla \phi[\mathbf{x}(t)]. \quad (2)$$

If we consider a non-uniform time-dependent flow which is inhomogeneous in space over scales much larger than $v_{ph}\tau_{rel}$ and varies in time over time-scales much larger than τ_{rel} then the particle in the fluid is locally in quasi-equilibrium state with uniform velocity $\mathbf{u}[t, \mathbf{x}(t)]$ so that

$$\mathbf{v}_{ph}(t) \approx \mathbf{u}[t, \mathbf{x}(t)] + c_{ph}[t, \mathbf{x}(t)] \nabla \phi[t, \mathbf{x}(t)]. \quad (3)$$

This result assumes that the reaction of the particle to the flow around it is local and that the local flow is constant on the particle scale. Thus the fluid does not have to be infinite but the boundaries, breaking the Galilean invariance, have to be far away.

We demonstrate how the consequence of locality and Galilean invariance (Eq. 3) can be obtained using concrete models. In many situations the force on the particle from the flow can be described by linear drag [4], implying that $\tau_{rel} \times d\mathbf{v}/dt = \mathbf{u} - \mathbf{v} + c_{ph} \nabla \phi$ where the combination $\mathbf{u} - \mathbf{v}$ is the consequence of Galilean invariance. The diffusiophoretic force is written so that it agrees with

Phoresis type	Driving gradient field ϕ ,	Phoretic velocity \mathbf{v}_{ph}	Compressibility $\nabla \cdot \mathbf{v}$, $\mathbf{v} = \mathbf{u} + \mathbf{v}_{ph}$
Thermophoresis	temperature T	$c_T \nabla T$	$c_T \nabla^2 T + \nabla c_T \cdot \nabla T$
Diffusiophoresis	concentration of chemical species, salinity C	ionic: $D_p \nabla \ln C$ nonionic: $D'_p \nabla C$	$D_p \nabla^2 \ln C$ $D'_p \nabla^2 C + \nabla D'_p \cdot \nabla C$
Electrophoresis	electric potential φ	$-c_E \nabla \varphi$	$-c_E \nabla^2 \varphi - \nabla c_E \cdot \nabla \varphi$
Chemotaxis	chemical attractant concentration, ν	$\chi(\nu) \nabla \nu$	$\chi \nabla^2 \nu + \chi' [\nabla \nu]^2$
Phoretic particles concentrate on a multi-fractal described by $\langle n(\mathbf{x})n(\mathbf{x} + \mathbf{r}) \rangle = \langle n(\mathbf{x}) \rangle \langle n(\mathbf{x} + \mathbf{r}) \rangle (\eta/r)^\Delta$, $\Delta > 0$; $\Delta = \int_{-\infty}^{\infty} \langle \nabla \cdot \mathbf{v}(0) \nabla \cdot \mathbf{v}(t) \rangle dt / \lambda_3 $ is twice the ratio of logarithmic rates of growth of infinitesimal volumes and areas.			

TABLE I: Description of clustering of phoretic particles in turbulence. The first column describes the phoretic phenomenon, the second column describes the field causing phoresis, the third column gives the phoretic velocity \mathbf{v}_{ph} for motion in the gradient of corresponding field. The fourth column provides the expression for the compressibility $\nabla \cdot \mathbf{v}$, where $\mathbf{v} = \mathbf{u} + \mathbf{v}_{ph}$. The last row is the prediction of clustering described by the pair-correlation function of concentration n .

\mathbf{v}_{ph} in the case $\mathbf{u} = 0$. This expression also describes the cases where the Reynolds number of the motion of the particle with respect to the flow is not too small, see [39] and references therein. In the limit of small particle relaxation time $\tau \rightarrow 0$ we recover $\mathbf{v} = \mathbf{u} + c_{ph} \nabla \phi$.

We sketch how the limitations of Eq. (3) could be studied for the case of diffusiophoresis. We consider the velocity $\mathbf{v}(t)$ of a diffusiophoretic particle in the flow $\mathbf{u}(t, \mathbf{x})$ with salinity concentration $C(t, \mathbf{x})$. The fields can be coupled (for instance with coupling described with Boussinesq equations below) or not. If both $\mathbf{u}(t, \mathbf{x})$ and $C(t, \mathbf{x})$ vary over spatial scales much larger than the typical value of $\tau_{rel} D_p |\nabla \ln C|$ and over temporal scales much larger than τ_{rel} then,

$$\mathbf{v}(t) \approx \mathbf{u}[t, \mathbf{x}(t)] + D_p \nabla \ln C[t, \mathbf{x}(t)], \quad (4)$$

cf. Eq. (3). We demonstrate briefly how fluid mechanics confirms this. We consider the typical situation where the interaction of the turbulent flow with the field C can be described using the Boussinesq approximation,

$$\begin{aligned} \partial_t \mathbf{u} + \mathbf{u} \cdot \nabla \mathbf{u} &= -\nabla p + C \mathbf{g} + \nu \nabla^2 \mathbf{u}, \quad \nabla \cdot \mathbf{u} = 0, \\ \partial_t C + \mathbf{u} \cdot \nabla C &= D_S \nabla^2 C, \end{aligned} \quad (5)$$

where p is pressure divided by density, D_S is the diffusivity coefficient and ν is the kinematic viscosity of the fluid. We use a rescaled field C so that the buoyancy force is $C \mathbf{g}$ where \mathbf{g} is the gravitational acceleration. This is possible because the equation on C and the phoretic velocity $D_p \ln C$ in Eq. (4) do not change when C is rescaled by a constant. The phoretic particle is represented through the boundary conditions on the particle's surface $|\mathbf{x} - \mathbf{x}(t)| = a$ where for definiteness we consider a ball with small radius a . The boundary conditions include finite corrections to no-slip boundary conditions necessary for the fluid mechanical description of the phoresis [3]. We write the flow as sum of $\mathbf{u}(t, \mathbf{x})$ plus the perturbation flow $\mathbf{u}'[t, \mathbf{x} - \mathbf{x}(t)]$ centered at the moving position of the particle. The perturbation flow

designated by primes obeys the linearized fluid mechanical equations,

$$\begin{aligned} \partial_t \mathbf{u}' + [\mathbf{u} - \mathbf{v}] \cdot \nabla \mathbf{u}' + \mathbf{u}' \cdot \nabla \mathbf{u} &= -\nabla p' + C' \mathbf{g} + \nu \nabla^2 \mathbf{u}', \\ \partial_t C' + [\mathbf{u} - \mathbf{v}] \cdot \nabla C' + \mathbf{u}' \cdot \nabla C &= D_S \nabla^2 C', \quad \nabla \cdot \mathbf{u}' = 0, \end{aligned}$$

where the boundary conditions on the perturbation flow are those in the rest frame minus the local value of the flow $\mathbf{u}[t, \mathbf{x}(t)]$. Here we neglect the variation of $\mathbf{u}(t, \mathbf{x})$ over the scale of the particle. Further, smallness of the particle's temporal and spatial scales compared with those of the flow implies that the LHS of equations on \mathbf{u}' , C' can be neglected giving

$$\begin{aligned} 0 &= -\nabla p' + C' \mathbf{g} + \nu \nabla^2 \mathbf{u}', \quad \nabla \cdot \mathbf{u}' = 0, \\ 0 &= D_S \nabla^2 C'. \end{aligned} \quad (6)$$

Thus we find the equations for the perturbation flow that coincide with those in the fluid that moves at the uniform constant velocity whose value is $\mathbf{u}[t, \mathbf{x}(t)]$. The solution is Eq. (4) where we neglect other forces such as fluid acceleration, added mass and Basset ones [4]. These are negligible in the usual situations of phoresis and whose consideration is beyond our study here. Other cases of phoretic phenomena are easily obtained by renaming the letters, see table I and section VII.

The phoretic component of the flow causes finite compressibility due to the drift:

$$\nabla \cdot \mathbf{v} = \nabla \cdot \mathbf{v}_{ph} = \nabla c_{ph} \cdot \nabla \phi + c_{ph} \nabla^2 \phi, \quad (7)$$

indicating that compressibility effects are produced by the inhomogeneity of $\nabla \phi$ or inhomogeneity of the phoretic coefficient c_{ph} . The last column of Table I lists the form of the compressibility $\nabla \cdot \mathbf{v}$ for the most common types of phoresis. The fact that $\nabla \cdot \mathbf{v} \neq 0$ for phoretic particles is the process that leads to clustering onto a multifractal set, as will be elaborated in the next section.

The flow field \mathbf{u} and scalar field ϕ evolve according to

$$\begin{aligned}\partial_t \mathbf{u} + \mathbf{u} \cdot \nabla \mathbf{u} &= -\nabla p + \nu \nabla^2 \mathbf{u} + \mathbf{f}(\phi), \quad \nabla \cdot \mathbf{u} = 0, \\ \partial_t \phi + \mathbf{u} \cdot \nabla \phi &= D_\phi \nabla^2 \phi,\end{aligned}\quad (8)$$

where p is the kinematic pressure, ν is the kinematic viscosity of the fluid and D_ϕ is the diffusivity of ϕ . Here, $\mathbf{f}(\phi)$ is a body force induced by ϕ . If $\mathbf{f} = \mathbf{0}$, the scalar is passive, and if $\mathbf{f} \neq \mathbf{0}$ the scalar is active. For the Navier-Stokes equations in the Boussinesq approximation, the body force is given by $\mathbf{f} = \hat{\rho} \mathbf{g}$ where $\hat{\rho}$ is an equation of state linking ϕ to the normalised density; two examples being when ϕ represents the salinity C [in the case of diffusiophoresis, see Eq. (8)] or temperature T (in the case of thermophoresis).

The ratio of the kinematic viscosity ν to the diffusivity D_ϕ is referred to as the Schmidt number Sc in case ϕ is a solute and as the Prandtl number Pr when the scalar under consideration is the temperature. In the discussion below, Sc will be used but the arguments are identical for Pr . The smallest scale of variations in \mathbf{u} when the flow is turbulent is the Kolmogorov length scale $\eta = \sqrt{\nu/\lambda}$ where $\lambda = \sqrt{\epsilon/\nu}$ is the typical value of velocity gradients of turbulence (inverse Kolmogorov time-scale) and ϵ is turbulent kinetic energy dissipation rate per unit volume. This is the scale at which the non-linearity $\mathbf{u} \cdot \nabla \mathbf{u}$ and the viscous term $\nu \nabla^2 \mathbf{u}$ in Eq. (8) balance each other [1]. The counterpart of η for the scalar field ϕ , i.e. the smallest scale l_d of variations of ϕ at which $\mathbf{u} \cdot \nabla \phi$ and $D_\phi \nabla^2 \phi$ balance, depends on the Schmidt number $Sc = \nu/D_\phi$. In typical oceanic applications and the experiment described in Section VII we have $Sc \sim 10^3$. In this case l_d is the Batchelor scale $\sqrt{D_S/\lambda}$ which is much smaller than η so the flow in the range $l_d \ll r \ll \eta$ is differentiable with fluctuations of velocity at scales r of order λr . The variance of ϕ is cascaded by smooth flow from η to l_d where it is stopped by diffusion [54]. The Batchelor scale is the scale where diffusion balances the local shrinking of filaments of salinity by gradients of the flow and this is the typical scale of variations of ϕ in oceanic flows. In this case the correlation scale l_d of gradients of ϕ is much smaller than that of gradients of \mathbf{u} . The correlation scale of gradients of the flow of particles in Eq. (3) is l_d . In the case where Sc is of order one or smaller the correlation length of gradients of ϕ is of order η so that the correlation scale of gradients of the flow of particles is given by the correlation scale η of $\nabla \mathbf{u}$. Thus we introduce the correlation scale $l_0 = \min[\sqrt{\nu/\lambda}, \sqrt{D_\phi/\lambda}]$ of gradients of \mathbf{v} that holds independently of Sc .

III. PHORETIC CLUSTERING IN TURBULENCE

In this section we demonstrate theoretically that phoretic particles cluster in turbulence. We introduce a universal framework for different phoretic phenomena including thermophoresis, electrophoresis, chemotaxis and

diffusiophoresis, see Table I. Other cases where our predictions have potential applications are barophoresis and pycnophoresis, see [55] and references therein. This universality is possible because clustering of phoretic particles in turbulence is a direct consequence of fractality of the distribution of particles in weakly compressible random flows and Galilean invariance of fluids.

As argued in the previous section, the motion of a phoretic particle with coordinate $\mathbf{x}(t)$ in a turbulent flow $\mathbf{v}(t, \mathbf{x})$ is governed by

$$\frac{d\mathbf{x}}{dt} = \mathbf{v}[t, \mathbf{x}(t)], \quad \mathbf{v} = \mathbf{u} + c_{ph} \nabla \phi, \quad (9)$$

see Eq. (3). The condition of validity of this description is that the scale of spatial variations of ϕ is much larger than the particle's size, $\lambda \tau_{rel} \ll 1$ and $v_{ph} \tau_{rel} \ll l_0$ where v_{ph} is the typical value of the phoretic velocity $c_{ph} |\nabla \phi|$.

We consider the case where the particles' flow has weak compressibility so the flow divergence is much smaller than the typical value of the gradients of turbulence,

$$|\nabla \cdot (c_{ph} \nabla \phi)| \ll \lambda. \quad (10)$$

Using that $|\nabla \cdot (c_{ph} \nabla \phi)| \sim |c_{ph} \nabla \phi|/l_0 \sim v_{ph}/l_0$ we find that the condition of weak compressibility is,

$$v_{ph} \ll \lambda l_0. \quad (11)$$

We observe that $|\nabla \cdot (c_{ph} \nabla \phi)|/\lambda = (v_{ph} \tau_{rel}/l_0)(\lambda \tau_{rel})^{-1}$; that is, the validity of conditions (10)-(11) is determined by which of the two small numbers $\lambda \tau_{rel}$, $v_{ph} \tau_{rel}/l_0$ is smaller.

The weak compressibility of the particles' flow implies that the particles' distribution in space can be described completely using the universal description of statistics of particle distribution in weakly compressible flow that was introduced in [6, 19]. It was demonstrated in [19] that in the steady state the particles concentrate on a random time-dependent multi-fractal in space. The statistics of the particles concentration field $n(t, \mathbf{x})$ is log-normal so that the correlation functions derive from the pair correlation function

$$\langle n(0)n(\mathbf{r}) \rangle = \langle n \rangle^2 \left(\frac{\eta}{r} \right)^\Delta, \quad r \ll l_0, \quad (12)$$

$$\langle n(\mathbf{x}_1)n(\mathbf{x}_2) \dots n(\mathbf{x}_k) \rangle = \prod_{i>k} \langle n(\mathbf{x}_i)n(\mathbf{x}_k) \rangle, \quad (13)$$

where Δ is the correlation codimension of the fractal that is given by

$$\Delta = \frac{1}{|\lambda_3|} \int_{-\infty}^{\infty} \langle \nabla \cdot [c_{ph} \nabla \phi](0) \nabla \cdot [c_{ph} \nabla \phi](t) \rangle dt, \quad (14)$$

where $|\lambda_3|$ is the Lyapunov exponent associated with the growth exponent of infinitesimal areas, see below.

Equation (14) is the main result of this section: phoretic particles form a multifractal in turbulent flow with log-normal statistics determined by Eqs. (12)-(14),

see table I. Logically, this is what we will base further calculations and our experimental validation in section VII on.

In the following we clarify and discuss these results. The correlation codimension Δ coincides with twice the Kaplan-Yorke codimension D_{KY}

$$\Delta = 2D_{KY}, \quad (15)$$

whose definition [56] in the case of weak compressibility reduces to the ratio of logarithmic growth rates of infinitesimal volumes δV and areas δA of particles [39],

$$D_{KY} = \left| \lim_{t \rightarrow \infty} \frac{1}{t} \ln \left(\frac{\delta V(t)}{\delta V(0)} \right) \right| \left| \lim_{t \rightarrow \infty} \frac{1}{t} \ln \left(\frac{\delta A(t)}{\delta A(0)} \right) \right|^{-1}. \quad (16)$$

The weak compressibility causes this to be much smaller than one: for incompressible flow the volumes are conserved but the areas grow with finite exponent when the flow is chaotic (which the turbulent flow below the Kolmogorov scale is). The limits in D_{KY} hold deterministically involving no averaging because the limiting rates coincide for different initial positions of volumes and areas. The limit for the volume is called the sum of the Lyapunov exponents λ_i ,

$$\begin{aligned} \sum \lambda_i &= \lim_{t \rightarrow \infty} \frac{1}{t} \ln \left(\frac{\delta V(t)}{\delta V(0)} \right) \\ &= - \int_0^\infty \langle \nabla \cdot [c_{ph} \nabla \phi](0) \nabla \cdot [c_{ph} \nabla \phi](t) \rangle dt, \quad (17) \end{aligned}$$

where we use the formula for $\sum \lambda_i$ derived in [57]. The three Lyapunov exponents are ordered such that $\lambda_1 > \lambda_2 > \lambda_3$, and we note that for fluid particles ($\nabla \cdot \mathbf{u} = 0$) we would have $\sum \lambda_i = 0$. The negative sign of $\sum \lambda_i$ indicates that particles migrate to regions with negative flow divergence, see the discussion in the next Section. If we consider four infinitesimally separated particles, the volume $\delta V(t)$ of the tetrahedron that they form will decrease at large times exponentially at the rate $\sum \lambda_i$ identical for different initial positions of the particles and different initial times. Since the correlation time of $\nabla \cdot \mathbf{v}$ is the Kolmogorov time-scale then we find,

$$\frac{\sum \lambda_i}{\lambda} \sim \frac{v_{ph}^2}{l_0^2 \lambda^2} \ll 1, \quad (18)$$

where we used Eq. (11). The logarithmic rate of growth of infinitesimal areas δA is non-zero for fluid particles so that using the smallness of the phoretic component of the flow we can use in Eq. (16) the Lagrangian trajectories of the fluid particles (this approximation would fail for $\sum \lambda_i$ because that is zero for turbulence). For fluid particles volumes are conserved so that the growth exponent of infinitesimal areas coincides with the third Lyapunov exponent (see the next Section),

$$|\lambda_3| = \lim_{t \rightarrow \infty} \frac{1}{t} \ln \left(\frac{\delta A(t)}{\delta A(0)} \right), \quad (19)$$

where the simplest configuration that determines $|\lambda_3|$ is the triangle formed by three infinitesimally close fluid particles. The area of the triangle growth becomes at large times deterministic with exponent given by $|\lambda_3|$ identical for all triangles. There is no simple way of writing $|\lambda_3|$ in terms of correlation functions of turbulence so it has to be considered as phenomenological positive quantity of order λ so that,

$$D_{KY} = \frac{|\sum \lambda_i|}{|\lambda_3|} \sim \frac{\sum \lambda_i}{\lambda} \sim \frac{v_{ph}^2}{l_0^2 \lambda^2} \ll 1. \quad (20)$$

The averages in Eq. (12)-(14) are spatial,

$$\langle n(0)n(\mathbf{r}) \rangle = \int n(\mathbf{x})n(\mathbf{x} + \mathbf{r}) \frac{d\mathbf{x}}{\Omega}, \quad (21)$$

$$\begin{aligned} \langle \nabla \cdot [c_{ph} \nabla \phi](0) \nabla \cdot [c_{ph} \nabla \phi](t) \rangle &= \int \nabla \cdot [c_{ph} \nabla \phi](0, \mathbf{x}) \\ \nabla \cdot [c_{ph} \nabla \phi][t, \mathbf{q}(t, \mathbf{x})] \frac{d\mathbf{x}}{\Omega}, \quad (22) \end{aligned}$$

where Ω is the total volume which is set below to one and we introduced the spatial Lagrangian trajectories of the fluid particles labeled by their position at $t = 0$

$$\partial_t \mathbf{q}(t, \mathbf{x}) = \mathbf{u}[t, \mathbf{q}(t, \mathbf{x})], \quad \mathbf{q}(t = 0, \mathbf{x}_0) = \mathbf{x}_0. \quad (23)$$

The described predictions hold for spatially uniform statistics of turbulence provided $\Delta \ll 1$. The case of inhomogeneous statistics is considered in the next Section.

We comment on the validity of Eq. (14). The original formula for the average in the pair-correlation function (Eq. 22) in Δ does not involve the trajectories of the fluid particles $\mathbf{q}(t, \mathbf{x})$ but the trajectories of the phoretic particles $\mathbf{x}(t, \mathbf{x})$,

$$\partial_t \mathbf{x}(t, \mathbf{x}) = \mathbf{v}[t, \mathbf{x}(t, \mathbf{x})], \quad \mathbf{x}(t = 0, \mathbf{x}_0) = \mathbf{x}_0. \quad (24)$$

defined by \mathbf{v} and not \mathbf{u} , see [19]. However condition (11) implies that ($l_0 \leq \eta$)

$$\frac{v_{ph}}{\lambda \eta} \leq \frac{v_{ph}}{\lambda l_0} \ll 1, \quad (25)$$

that is, the typical value of the phoretic velocity is much smaller than the typical value $\lambda \eta$ of the turbulent velocity at the scale η . Thus during the Lagrangian correlation time λ^{-1} of turbulent velocity gradients in the fluid particle's frame the phoretic particle deviates from the fluid particle by a distance much smaller than the correlation scale of the gradients η that is $|\mathbf{q}(t = \lambda^{-1}, \mathbf{x}) - \mathbf{x}(t = \lambda^{-1}, \mathbf{x})| \ll \eta$. Thus over the correlation time λ^{-1} which determines the time integral in Eq. (14) the gradients in the fluid's and phoretic particle's frames coincide so we can use $\mathbf{q}(t, \mathbf{x})$ instead of $\mathbf{x}(t, \mathbf{x})$ in Eq. (22).

IV. PREFERENTIAL CONCENTRATION IN INHOMOGENEOUS TURBULENCE

In this Section we derive the pair-correlation function $\langle n(\mathbf{x})n(\mathbf{x} + \mathbf{r}) \rangle$ of the concentration field $n(t, \mathbf{x})$ of par-

ticles in the case where the statistics of turbulence is inhomogeneous. We find a universal formula for pair correlations of particles in inhomogeneous weakly compressible random flow. Though different inhomogeneities of the flow produce different spatial profiles $n_0(\mathbf{x})$ of average concentration $\langle n(\mathbf{x}) \rangle = n_0(\mathbf{x})$ we demonstrate that fluctuations of normalized concentration,

$$\tilde{n}(t, \mathbf{x}) = \frac{n(t, \mathbf{x})}{n_0(\mathbf{x})}, \quad (26)$$

obey universal statistics. These coincide with those of concentration for spatially uniform statistics described in the previous Section. We find that $\tilde{n}(t, \mathbf{x})$ has log-normal statistics (13) which is completely determined by the pair-correlation function

$$\langle \tilde{n}(\mathbf{x}) \tilde{n}(\mathbf{x} + \mathbf{r}) \rangle = \left(\frac{l_0}{r} \right)^{\Delta(\mathbf{x} + \mathbf{r}/2)}, \quad r \ll l_0, \quad (27)$$

where the difference from the spatially uniform case is that Δ is a function of the coordinate that reflects inhomogeneity of the velocity statistics,

$$\Delta = \frac{1}{|\lambda_3(\mathbf{x})|} \int_{-\infty}^{\infty} dt \langle \nabla \cdot [c_{ph} \nabla \phi](0) \nabla \cdot [c_{ph} \nabla \phi](t) \rangle(\mathbf{x}) \quad (28)$$

Thus describing the statistics of concentration of phoretic particles in inhomogeneous turbulence reduces to the problem of determining the concentration profile $n_0(\mathbf{x})$ and $\Delta(\mathbf{x})$ provided the weak compressibility condition (11) holds. In this work we concentrate on deriving Eq. (27) considering $n_0(\mathbf{x})$ and $\Delta(\mathbf{x})$ as phenomenological fields determined by the details of statistics of turbulence. The study of how $n_0(\mathbf{x})$ can be obtained from the statistics of turbulence is undertaken in [58].

The pair-correlation function of concentration describes the probability to find a particle at distance \mathbf{r} from a particle at \mathbf{x} so that it enters the collision kernel determining the rate of coagulation of colloids having direct practical applications. In inhomogeneous cases the probability depends both on \mathbf{r} and \mathbf{x} . Thus the statistics are defined by time averaging,

$$\langle n(\mathbf{x}) n(\mathbf{x} + \mathbf{r}) \rangle = \lim_{t_0 \rightarrow \infty} \frac{1}{t_0} \int_0^{t_0} n(t, \mathbf{x}) n(t, \mathbf{x} + \mathbf{r}) dt, \quad (29)$$

$$n_0(\mathbf{x}) = \langle n(\mathbf{x}) \rangle = \lim_{t_0 \rightarrow \infty} \frac{1}{t_0} \int_0^{t_0} n(t, \mathbf{x}) dt. \quad (30)$$

The pair-correlation function can be obtained as the probability $\langle n(\mathbf{x}) \rangle$ of finding a particle at \mathbf{x} times the conditional probability $P(\mathbf{x}|\mathbf{r})$ of finding a particle at $\mathbf{x} + \mathbf{r}$ given that there is a particle at \mathbf{x} (here the angular brackets stand for temporal averaging at fixed spatial positions, see definitions below). When r gets large the location of the particle at \mathbf{x} does not influence the probability $P(\mathbf{x}|\mathbf{r})$ of finding a particle at $\mathbf{x} + \mathbf{r}$ so that $P(\mathbf{x}|\mathbf{r}) \approx \langle n(\mathbf{x} + \mathbf{r}) \rangle$ and $\langle n(\mathbf{x}) n(\mathbf{x} + \mathbf{r}) \rangle \approx \langle n(\mathbf{x}) \rangle \langle n(\mathbf{x} + \mathbf{r}) \rangle$. Thus at large separations the pair-correlation function decomposes to the product of averages describing independence

of concentration fluctuations at separated points. In contrast, when $r \rightarrow 0$ there is an increase in $P(\mathbf{x}|\mathbf{r})$ reflecting particles clustering together in preferred regions of the flow - preferential concentration. It is this increase factor,

$$f(\mathbf{x}, \mathbf{r}) = \frac{\langle n(\mathbf{x}) n(\mathbf{x} + \mathbf{r}) \rangle}{\langle n(\mathbf{x}) \rangle \langle n(\mathbf{x} + \mathbf{r}) \rangle} = \langle \tilde{n}(\mathbf{x}) \tilde{n}(\mathbf{x} + \mathbf{r}) \rangle, \quad (31)$$

which we derive in this Section. This factor is a "proper correlation": if $n_0(\mathbf{x})$ is larger in certain regions of space then particles will tend to go to that region independently of the behavior of other particles so the product $n(\mathbf{x}) n(\mathbf{x} + \mathbf{r})$ will be larger there trivially. Our derivation holds for arbitrary weakly compressible flow so that it can be used for all the phoretic phenomena described in the previous Section, inertial particles in turbulence at small Stokes or Froude numbers [19, 39] or other cases.

The reasons why turbulence increases the probability of two particles to get close can be understood from the fact that on average the divergence of velocity in the particle's frame is negative $\langle \nabla \cdot \mathbf{v}[t, \mathbf{x}(t, \mathbf{x})] \rangle < 0$. Particles tend to go to regions where the divergence is negative so in the particle's frame the divergence is mostly negative. Thus when two particles transported by turbulence are randomly brought below the "minimal correlation length" of velocity divergence l'_0 they start moving in the same divergence which is typically negative. Motion in common divergence causes the particles to preferentially approach each other producing $f(\mathbf{x}, \mathbf{r}) > 1$, see Fig. 1. Here l'_0 is the largest scale over which $\nabla \mathbf{v}$ can be considered constant which can be taken one order of magnitude smaller than l_0 . We will demonstrate that there is no correlation of concentration fluctuations at l'_0 .

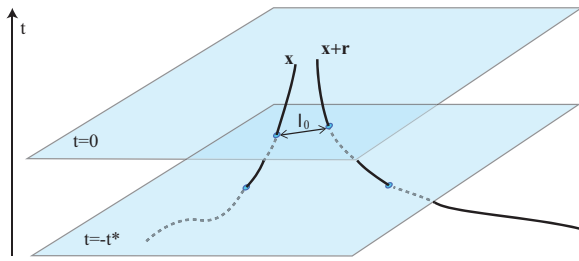
We consider an increase in the probability of two particles carried along by turbulence to approach each other at distance $r \ll l'_0$ at the time of observation $t = 0$ which is described by the pair-correlation function. We can separate the history of the particles' motion in space at $t < 0$ to times $t < t_*$ when the particles' separation $r(t)$ was larger than l'_0 and times $t_* < t < 0$ where $r(t) < l'_0$, see Fig. 1. The particles' moved in uncorrelated divergences of the flow at $t < t_*$ so there was no preference to getting closer or further (the residual power-law correlations in the inertial range have small but finite value which we study below. These are not relevant for finding the leading order term here). The increase in probability is built in the last period of motion in the common velocity divergence. This can be described by using the continuity equation

$$\partial_t n + \nabla \cdot (n \mathbf{v}) = 0, \quad (32)$$

which has the solution $n(\mathbf{x}) = n[t = 0, \mathbf{x}]$,

$$n(\mathbf{x}) = n[t, \mathbf{x}(t, \mathbf{x})] \exp \left[- \int_t^0 \nabla \cdot \mathbf{v}[t', \mathbf{x}(t', \mathbf{x})] dt' \right] \quad (33)$$

where $\mathbf{x}(t, \mathbf{x})$ is the particle trajectory that passes at $t = 0$ through the point \mathbf{x} , see Eq. (24). We find taking the



$$\frac{\langle n(\mathbf{x})n(\mathbf{x}+\mathbf{r}) \rangle}{\langle n(\mathbf{x}) \rangle \langle n(\mathbf{x}+\mathbf{r}) \rangle} = \frac{\left\langle \exp \left[-2 \int_{-t^*}^0 dt \nabla \cdot \mathbf{v}[t, \mathbf{x}(t, \mathbf{x}+\mathbf{r}/2)] \right] \right\rangle}{\left\langle \exp \left[- \int_{-t^*}^0 dt \nabla \cdot \mathbf{v}[t, \mathbf{x}(t, \mathbf{x}+\mathbf{r}/2)] \right] \right\rangle^2}$$

FIG. 1: Illustration of turbulence’s formation of positive correlations in positions of phoretic particles. The particle on its own is found more often in regions with negative divergence of the flow because the particles flow to those regions. When random turbulent transport brings at time $-t^*$ another particle to a distance l_0 from the given particle, their common motion in the predominantly negative divergence of the flow creates effective attraction between the particles. The particles’ correlation at the time $-t^*$ is negligible because they moved in weakly correlated divergences at $t < -t^*$. The pair-correlation $\langle n(\mathbf{x})n(\mathbf{x}+\mathbf{r}) \rangle$ is the probability $\langle n(\mathbf{x}) \rangle \langle n(\mathbf{x}+\mathbf{r}) \rangle$ to randomly get close by distance l_0 times the increase factor due to common motion in the predominantly negative divergence which is the RHS of the formula at the bottom of the figure.

product of $n(\mathbf{x})$ and $n(\mathbf{x}+\mathbf{r})$ and averaging that,

$$\langle n(\mathbf{x})n(\mathbf{x}+\mathbf{r}) \rangle = \left\langle n[t, \mathbf{x}(t, \mathbf{x})]n[t, \mathbf{x}(t, \mathbf{x}+\mathbf{r})] \exp \left[- \int_t^0 dt' (\nabla \cdot \mathbf{v}[t', \mathbf{x}(t', \mathbf{x})] + \nabla \cdot \mathbf{v}[t', \mathbf{x}(t', \mathbf{x}+\mathbf{r})]) \right] \right\rangle, \quad (34)$$

We demonstrated that pair correlations form when the distance between the particles is much less than l'_0 . We consider $r \ll l'_0$ and track the trajectories $\mathbf{x}(t, \mathbf{x})$ and $\mathbf{x}(t, \mathbf{x}+\mathbf{r})$ back in time in order to determine the positive correlation accumulated during the times when the distance $\mathbf{r}(t) = \mathbf{x}(t, \mathbf{x}+\mathbf{r}) - \mathbf{x}(t, \mathbf{x})$ between the trajectories was less than l'_0 .

We briefly sketch the properties of evolution of distances below the Kolmogorov scale, see [59–62] for details. The separation velocity is linear in \mathbf{r} at $r < l'_0$ because the particles’ velocity difference can be approximated by separation \mathbf{r} times the local flow gradient. Thus the separation below l'_0 is exponential. It is characterized by a positive exponent describing chaoticity of motion of particles below l'_0 ,

$$\lim_{t \rightarrow -\infty} \frac{1}{|t|} \ln \left(\frac{r(t)}{r(0)} \right) \approx |\lambda_3|, \quad (35)$$

where λ_3 is the third Lyapunov exponent of the fluid particles in turbulence. Thus at large times the growth of distances between trajectories back in time is deterministic exponential growth with exponent $|\lambda_3|$. This exponent can be seen in the forward in time evolution of

an infinitesimal ball of fluid particles with size r_0 much less than η . Turbulence deforms the ball to an ellipsoid whose axes behave exponentially [59–62]. The major axis increases as $r_0 \exp[\lambda_1 t]$ where $\lambda_1 > 0$ is the principal Lyapunov exponent. The minor axis decreases as $r_0 \exp[\lambda_3 t]$ where $\lambda_3 < 0$ is the third Lyapunov exponent. The exponential evolution of the intermediate axis $r_0 \exp[\lambda_2 t]$ is determined by the volume conservation condition $\lambda_1 + \lambda_2 + \lambda_3 = 0$. Then the growth of the distance between two fluid particles is given by λ_1 ,

$$\lim_{t \rightarrow \infty} \frac{1}{t} \ln \left(\frac{r(t)}{r(0)} \right) \approx \lambda_1, \quad (36)$$

which is the forward in time counterpart of Eq. (35). This holds at times much larger than the correlation time λ^{-1} of flow gradients which determine the velocity difference of close particles constituting form of ergodic theorem or the law of large numbers [59–62]. When evolution is time-reversed the major axis of the ellipsoid starts to grow at the exponent $|\lambda_3|$. Thus it is $|\lambda_3|$ that gives the logarithmic rate of separation of fluid particles back in time, see Eq. (35). The rate of separation of phoretic particles approximately coincides with $|\lambda_3|$ because the phoretic component of velocity is small. Thus Eq. (35) holds for both fluid and phoretic particles.

We conclude that when $r \rightarrow 0$ the time

$$t^* = \frac{1}{|\lambda_3|} \ln \left(\frac{l'_0}{r} \right), \quad (37)$$

that exponentially diverging trajectories $\mathbf{x}(t, \mathbf{x})$ and $\mathbf{x}(t, \mathbf{x}+\mathbf{r})$ spend below l'_0 grows logarithmically getting infinite at $r = 0$. This is because turbulence is smooth below η . The pair-correlations form at $r = 0$ for infinite time causing the divergence of $\langle n^2(\mathbf{x}) \rangle$, see below.

If turbulence is inhomogeneous then it is necessary to refine the considerations because the rate of separation λ_3 in this case depends on the position of the particles at $t = 0$. We consider the case which is typical in practice where the center of mass of the separating pair of particles stays in the region where the turbulent statistics is approximately uniform during the time interval $-t_* < t < 0$. In other words the scale L of inhomogeneity of turbulent statistics is assumed to be much larger than the typical distance $|\mathbf{x}(-t_*, \mathbf{x}) - \mathbf{x}|$. Since t^* diverges when $l \rightarrow 0$, see Eq. (37) then this implies that we consider not too small l . Then we can define

$$\frac{1}{t_*} \ln \left(\frac{|\mathbf{x}(-t_*, \mathbf{x}+\mathbf{r}) - \mathbf{x}(-t_*, \mathbf{x})|}{r} \right) \approx |\lambda_3(\mathbf{x})|, \quad (38)$$

that holds provided $\ln(l'_0/r) \gg 1$ or $|\lambda|t_* \gg 1$, see Eq. (37). The inequality guarantees that the LHS is the sum of $N \sim |\lambda|t_* \gg 1$ independent random variables divided by N so the law of large numbers holds defining a unique realization-independent function $\lambda_3(\mathbf{x})$. In practice the logarithm is never too large so our consideration is an asymptotic study which then is continued to the

physical range of parameters (the formulas that are derived under condition $\ln(l'_0/r) \gg 1$ hold when $l'_0/r \gg 1$). When we consider the decrease of l or increase in t^* the displacement $|\mathbf{x}(-t^*, \mathbf{x}) - \mathbf{x}|$ will reach L causing fluctuations in the LHS of Eq. (38). Further increase in t^* will produce the trajectory that explores the whole volume of the flow so that the LHS will become constant independent of the coordinate. The fluctuations of concentrations at not too small l are determined by $\lambda_3(\mathbf{x})$ when smaller r are probably unreachable practically and will not be studied in this work.

We observe that we consider the time t^* to separate from initial (or rather final) distance r to l'_0 as deterministic quantity. This neglects the fluctuations of finite-time Lyapunov exponents (large deviations [7, 61]). Consistent inclusion of the fluctuations demonstrates that those can be neglected because weakness of compressibility causes the averages to be determined by the most probable λ_3 and not the large deviations [19].

We consider Eq. (34) at $t = -t^*$. The average in the RHS contains both averaging over times smaller than $-t^*$ and the times of formation of pair correlations $-t^* < t < 0$. For separating these contributions we observe that the condition of weak compressibility (10) implies that time integral of $\nabla \cdot \mathbf{v}[t, \mathbf{x}(t, \mathbf{x})]$ over times of order of the correlation time λ^{-1} of $\nabla \cdot \mathbf{v}$ is much less than one (thus over these time-scales the concentration is conserved in the particle's frame,

$$n(\mathbf{x}) \approx n[t, \mathbf{x}(t, \mathbf{x})], \quad \lambda|t| \lesssim 1, \quad (39)$$

which is another way of describing weak compressibility of the flow). We find neglecting the contribution of times in λ^{-1} -vicinity of $-t^*$ that the concentration factors in the first line of Eq. (34) are independent of the exponential in the last line dependent on the "future flow",

$$\langle n(\mathbf{x})n(\mathbf{x} + \mathbf{r}) \rangle \approx \langle n[-t^*, \mathbf{x}(-t^*, \mathbf{x})]n[-t^*, \mathbf{x}(-t^*, \mathbf{x} + \mathbf{r})] \rangle \left\langle \exp \left[-2 \int_{-t^*}^0 dt \nabla \cdot \mathbf{v}[t, \mathbf{x}(t, \mathbf{x} + \mathbf{r}/2)] \right] \right\rangle,$$

where we used that $(\nabla \cdot \mathbf{v}[t, \mathbf{x}(t, \mathbf{x})]) \approx (\nabla \cdot \mathbf{v}[t, \mathbf{x}(t, \mathbf{x} + \mathbf{r})])$ for $-t^* < t < 0$ because the distance between the trajectories is much smaller than l_0 . We set the values of divergences at the trajectory issuing at the midpoint of \mathbf{x} and $\mathbf{x} + \mathbf{r}$ so that to have a symmetric form of the pair-correlation (the distinction between the points is beyond the accuracy of this calculation). Using that concentrations at distance l'_0 are not correlated (see below) we find,

$$\langle n(\mathbf{x})n(\mathbf{x} + \mathbf{r}) \rangle \approx \langle n[-t^*, \mathbf{x}(-t^*, \mathbf{x})] \rangle \langle n[-t^*, \mathbf{x}(-t^*, \mathbf{x} + \mathbf{r})] \rangle \left\langle \exp \left[-2 \int_{-t^*}^0 dt \nabla \cdot \mathbf{v}[t, \mathbf{x}(t, \mathbf{x} + \mathbf{r}/2)] \right] \right\rangle, \quad (40)$$

see Fig. 1. Finally dividing the equation by its counterpart for $\langle n(\mathbf{x}) \rangle$,

$$\langle n(\mathbf{x}) \rangle = \langle n[-t^*, \mathbf{x}(-t^*, \mathbf{x})] \rangle \left\langle \exp \left[-\int_{-t^*}^0 dt \nabla \cdot \mathbf{v}[t, \mathbf{x}(t, \mathbf{x})] \right] \right\rangle,$$

where we can use $\mathbf{x}(t, \mathbf{x} + \mathbf{r}/2)$ instead of $\mathbf{x}(t, \mathbf{x})$ we find,

$$f(\mathbf{x}, \mathbf{r}) = \frac{\left\langle \exp \left[-2 \int_{-t^*}^0 dt \nabla \cdot \mathbf{v}[t, \mathbf{x}(t, \mathbf{x} + \mathbf{r}/2)] \right] \right\rangle}{\left\langle \exp \left[-\int_{-t^*}^0 dt \nabla \cdot \mathbf{v}[t, \mathbf{x}(t, \mathbf{x} + \mathbf{r}/2)] \right] \right\rangle^2} \quad (41)$$

This describes a positive correlation as accumulation of density increases due to motion in the same velocity divergence normalized by the accumulation that would occur due to motion in uncorrelated divergences. The latter determines $n_0(\mathbf{x})$ but does not describe the "proper correlation" $f(\mathbf{x}, \mathbf{r})$.

Since compressibility is small then we can find the averages in the RHS of Eq. (41) using the Gaussian averaging formula $\ln \langle \exp[x] \rangle = \langle x \rangle + \langle x^2 \rangle_c / 2$ where $\langle x^2 \rangle_c = \langle x^2 \rangle - \langle x \rangle^2$ is the dispersion (this neglects higher order cumulants of third order and higher in compressibility [19, 63]). We find

$$f(\mathbf{x}, \mathbf{r}) = \exp \left[t^* \int_{-\infty}^{\infty} \langle \nabla \cdot \mathbf{v}(0) \nabla \cdot \mathbf{v}(t) \rangle(\mathbf{x}) dt \right], \quad (42)$$

where we used that t^* is much larger than the correlation time λ^{-1} of $\nabla \cdot \mathbf{v}$, see Eq. (37), and defined

$$\langle \nabla \cdot \mathbf{v}(0) \nabla \cdot \mathbf{v}(t) \rangle(\mathbf{x}) = \lim_{t_0 \rightarrow \infty} \frac{1}{t_0} \int_0^{t_0} dt' \nabla \cdot \mathbf{v}(t', \mathbf{x}) \nabla \cdot \mathbf{v}[t' + t, \mathbf{q}(t' + t|t', \mathbf{x})]. \quad (43)$$

In the leading order in weak compressibility the definition uses the trajectories of the fluid (and not phoretic particles that pass through \mathbf{x} at time t' ,

$$\partial_t \mathbf{q}(t|t', \mathbf{x}) = \mathbf{u}[t', \mathbf{q}(t|t', \mathbf{x})], \quad \mathbf{q}(t = t'|t', \mathbf{x}) = \mathbf{x}, \quad (44)$$

cf. Eq. (23). Using the definition (37) of t^* in Eq. (42) we find

$$f(\mathbf{x}, \mathbf{r}) = \left(\frac{l'_0}{r} \right)^{\Delta(\mathbf{x} + \mathbf{r}/2)} \approx \left(\frac{l_0}{r} \right)^{\Delta(\mathbf{x} + \mathbf{r}/2)}, \quad (45)$$

with $\Delta(\mathbf{x})$ defined in Eq. (28). Finally using that $\Delta \ll 1$ we obtain $(l'_0/l_0)^\Delta \approx 1$ where $l_0/l'_0 \sim 10$ finding Eq. (27). This formula holds when $r \ll l_0$. In the case where the Batchelor scale is much smaller than the Kolmogorov one, the fluctuations of the concentration occur in much smaller regions of space than in the case of inertial particles. Continuation of formulas derived under the condition of large $\ln(l_0/r)$ to the range of large l_0/r is traditional in the range of smoothness of the flow starting from [54].

Similar considerations for higher-order correlation functions based on [19] demonstrate that the log-normal statistics hold for rescaled concentration,

$$\langle \tilde{n}(\mathbf{x}_1) \tilde{n}(\mathbf{x}_2) \dots \tilde{n}(\mathbf{x}_k) \rangle = \prod_{i>k} \langle \tilde{n}(\mathbf{x}_i) \tilde{n}(\mathbf{x}_k) \rangle. \quad (46)$$

Furthermore the use of considerations of [19], illustrated in Section VI, gives a deterministic solution and

log-normal statistics for the coarse-grained concentration $n_l(0, \mathbf{x})$ (cf. the next Section),

$$\frac{n_l(0, \mathbf{x})}{\langle n(\mathbf{x}) \rangle} = \exp\left(-\int_{-t^*}^0 \nabla \cdot \mathbf{v}[t, \mathbf{x}(t, \mathbf{x})] dt\right), \quad (47)$$

$$\frac{\langle n_l^k(\mathbf{x}) \rangle}{\langle n(\mathbf{x}) \rangle^k} = \left(\frac{l_0}{l}\right)^{\Delta(\mathbf{x})k(k-1)/2}, \quad (48)$$

where $n_l(t, \mathbf{x})$ is defined with the help of the number of particles $N_l(t, \mathbf{x}) = \int_{|\mathbf{x}-\mathbf{x}'| < l} n(t, \mathbf{x}') d\mathbf{x}'$ inside the ball of radius $l \ll l_0$ centered at \mathbf{x} ,

$$n_l(t, \mathbf{x}) = \frac{N_l(t, \mathbf{x})}{(4\pi l^3)/3}, \quad (49)$$

so that for continuous distributions $l \rightarrow 0$ defines the concentration field (for the considered fractal distributions there is no well-defined limit). For $k = 2$ Eq. (48) reproduces the scaling of the pair-correlation function because $\langle N_l^2(\mathbf{x}) \rangle = \int_{|\mathbf{x}-\mathbf{x}_1| < l, |\mathbf{x}-\mathbf{x}_2| < l} \langle n(t, \mathbf{x}_1)n(t, \mathbf{x}_2) d\mathbf{x}_1 d\mathbf{x}_2 \rangle$. In Section VI we refine this formula including discreteness of matter.

The derived pair-correlation implies that $\langle n(\mathbf{x})n(\mathbf{x} + \mathbf{r}) \rangle$ has very different scales of variation with \mathbf{x} and \mathbf{r} . The scale of variation with \mathbf{x} is that of the average density profile which is determined by the scale L of inhomogeneity of the statistics of turbulence. For spatially uniform statistics this dependence disappears. In contrast the dependence on \mathbf{r} is a fast dependence that happens in the narrow range of \mathbf{r} where the correlation function decays from infinite value at zero separation $\langle n^2(\mathbf{x}) \rangle = \infty$ to its large separation value $\langle n(\mathbf{x}) \rangle \langle n(\mathbf{x} + \mathbf{r}) \rangle$ at scales smaller than $l_0 \ll L$ (there are no fluctuations at scale l_0 because of $\Delta \ll 1$).

Regularization of the divergence of $\langle n^2(\mathbf{x}) \rangle$ is determined by the break down of the continuity equation (Eq. 32) at the smallest scales. The break down can be determined by Brownian motion of the particles that introduces a diffusion term $D\nabla^2 n$ in the RHS of Eq. (32), by finite size of the particles, by the finite difference of the phoretic constants of the particles (due to size and properties difference) or other small scale phenomena. Thus the divergent single-point dispersion $\langle n^2 \rangle$ predicted by the power-law dependence is regularized at small scales at possibly large but finite value. The corresponding fluctuations of single-point concentration can be large with $\langle n^2(\mathbf{x}) \rangle$ larger than $\langle n(\mathbf{x}) \rangle^2$ by orders of magnitude.

V. PAIR CORRELATIONS OUTSIDE THE SCALE OF SMOOTHNESS

In this Section we consider the pair correlation function of concentration at all separations including those outside l_0 . We use the consideration of [19] that represents the steady state of concentration as the outcome of infinite time evolution starting with arbitrary initial condition where the concentration evolves according to the

continuity equation. One starts with uniform initial condition $n(t = -T) = n_0$ in the remote past, finds $n(t = 0)$ and takes the steady state limit of infinite evolution time $T \rightarrow \infty$. Solving the continuity equation along the particles' trajectories $\mathbf{x}(t, \mathbf{x})$ defined in Eq. (24),

$$\begin{aligned} \frac{d}{dt} n[t, \mathbf{x}(t, \mathbf{x})] &= [\partial_t + \mathbf{v} \cdot \nabla] n(t, \mathbf{x})|_{\mathbf{x}=\mathbf{x}(t, \mathbf{x})} \\ &= -n[t, \mathbf{x}(t, \mathbf{x})] w[t, \mathbf{x}(t, \mathbf{x})], \quad w(t, \mathbf{x}) = \nabla \cdot \mathbf{v}(t, \mathbf{x}), \end{aligned} \quad (50)$$

we find,

$$n(0, \mathbf{x}) = n_0 \exp\left(-\int_{-T}^0 w[t, \mathbf{x}(t, \mathbf{x})] dt\right). \quad (51)$$

We find for the pair-correlation function taking the product of $n(0, \mathbf{x})$ and $n(0, \mathbf{x} + \mathbf{r})$,

$$\begin{aligned} \frac{\langle n(\mathbf{x})n(\mathbf{x} + \mathbf{r}) \rangle}{\langle n(\mathbf{x}) \rangle \langle n(\mathbf{x} + \mathbf{r}) \rangle} &= \frac{1}{\left\langle \exp\left(-\int_{-T}^0 w[t, \mathbf{x}(t, \mathbf{x})] dt\right) \right\rangle} \\ &\frac{\left\langle \exp\left[-\int_{-T}^0 (w[t, \mathbf{x}(t, \mathbf{x})] + w[t, \mathbf{x}(t, \mathbf{x} + \mathbf{r})]) dt\right] \right\rangle}{\left\langle \exp\left(-\int_{-T}^0 w[t, \mathbf{x}(t, \mathbf{x} + \mathbf{r})] dt\right) \right\rangle}. \end{aligned} \quad (52)$$

Using the cumulant expansion theorem for writing the averages we find that in the leading order in weak compressibility we can use the Gaussian approximation $\langle \exp[x] \rangle = \exp[\langle x \rangle + \langle x^2 \rangle_c / 2]$ in the averages [19, 63] which gives,

$$\begin{aligned} \frac{\langle n(\mathbf{x})n(\mathbf{x} + \mathbf{r}) \rangle}{\langle n(\mathbf{x}) \rangle \langle n(\mathbf{x} + \mathbf{r}) \rangle} &= \exp\left[\int_{-\infty}^0 dt_1 dt_2 \langle w[t_1, \mathbf{q}(t_1, \mathbf{x})] w[t_2, \mathbf{q}(t_2, \mathbf{x} + \mathbf{r})] \rangle\right] \end{aligned} \quad (53)$$

where we took the steady state limit $T \rightarrow \infty$ and used the fluid particles trajectories $\mathbf{q}(t, \mathbf{x})$ instead of $\mathbf{x}(t, \mathbf{x})$ in the leading order in weak compressibility, see Eqs. (23)-(24). This is a rigorous representation of the pair-correlation function in the limit of weak compressibility that was derived for spatially uniform statistics in [19]. The pair correlation function at $r \ll l_0$ is obtained by observing that at these scales the flow divergence w is identical at both trajectories up to times where the distance between the trajectories becomes comparable with the scale l_0 of spatial variations of $w(t, \mathbf{x})$. If $r \rightarrow 0$ then the trajectories coincide at all times so we find divergence in $\langle n^2(\mathbf{x}) \rangle$. When r is small but finite the leading order term is obtained considering how the time that the trajectories stay below l_0 diverges at small r . This is the time t^* that we studied in the previous Section,

$$\begin{aligned} &\int_{-\infty}^0 dt_1 dt_2 \langle w[t_1, \mathbf{q}(t_1, \mathbf{x})] w[t_2, \mathbf{q}(t_2, \mathbf{x} + \mathbf{r})] \rangle \\ &\approx t^* \int_{-\infty}^{\infty} dt_2 \langle w[t_1, \mathbf{q}(t_1, \mathbf{x})] w[t_2, \mathbf{q}(t_2, \mathbf{x})] \rangle, \quad r \ll l_0, \end{aligned} \quad (54)$$

which reproduces formula (42) for the pair correlation function obtained in the previous Section (the pair correlation function in the integral on the RHS depends on time difference $t_2 - t_1$ only because of incompressibility of flow of fluid particles). Beyond the scale $l'_0 \sim l_0/10$ the spatial correlations of concentration are weak so that $\langle n(\mathbf{x})n(\mathbf{x}+\mathbf{r}) \rangle \approx \langle n(\mathbf{x}) \rangle \langle n(\mathbf{x}+\mathbf{r}) \rangle$. This is reproduced by observing that at these scales the exponent in Eq. (53) is small because nothing compensates the smallness of compressibility (at smaller scales it is time of separation t^* that does the compensation). The leading order correction is obtained by expanding the exponent,

$$\frac{\langle n(\mathbf{x})n(\mathbf{x}+\mathbf{r}) \rangle}{\langle n(\mathbf{x}) \rangle \langle n(\mathbf{x}+\mathbf{r}) \rangle} - 1 \quad (55)$$

$$\approx \int_{-\infty}^0 dt_1 dt_2 \langle w[t_1, \mathbf{q}(t_1, \mathbf{x})] w[t_2, \mathbf{q}(t_2, \mathbf{x}+\mathbf{r})] \rangle, \quad r \gtrsim l'_0.$$

This formula holds for the Navier-Stokes turbulence involving no approximations so far. We provide estimates for the integral in the RHS. We observe that at scales $r \gtrsim l_0$ the pair-correlation function $\langle w(\mathbf{x})w(\mathbf{x}+\mathbf{r}) \rangle$ decays with r in contrast with $r \ll l_0$. Thus if we introduce the characteristic time t_r during which the separation of trajectories $\mathbf{q}(t_1, \mathbf{x})$, $\mathbf{q}(t_2, \mathbf{x}+\mathbf{r})$ grows by factor of order one then we have,

$$\frac{\langle n(\mathbf{x})n(\mathbf{x}+\mathbf{r}) \rangle}{\langle n(\mathbf{x}) \rangle \langle n(\mathbf{x}+\mathbf{r}) \rangle} - 1 \sim t_r^2 \langle w(\mathbf{x})w(\mathbf{x}+\mathbf{r}) \rangle, \quad r \gtrsim l'_0. \quad (56)$$

We disregarded the difference of time-scales of l'_0 and l_0 since it consists of logarithmic factor $\sim \ln 10$ which is of order one. The scaling produced depends on r/η . If we consider $r \lesssim \eta$ than in time of order λ^{-1} the trajectories separate by factor of order one so that we find,

$$\frac{\langle n(\mathbf{x})n(\mathbf{x}+\mathbf{r}) \rangle}{\langle n(\mathbf{x}) \rangle \langle n(\mathbf{x}+\mathbf{r}) \rangle} - 1 \sim \frac{\langle w(\mathbf{x})w(\mathbf{x}+\mathbf{r}) \rangle}{\lambda^2}, \quad l'_0 \lesssim r \lesssim \eta.$$

When scales $r \gg \eta$ are studied the characteristic separation time t_r of the trajectories separated initially (or rather finally) by r roughly obeys the Richardson scaling $t_r \sim r^{2/3} \epsilon^{-1/3}$ so that

$$\frac{\langle n(\mathbf{x})n(\mathbf{x}+\mathbf{r}) \rangle}{\langle n(\mathbf{x}) \rangle \langle n(\mathbf{x}+\mathbf{r}) \rangle} - 1 \sim r^{4/3} \epsilon^{-2/3} \langle w(\mathbf{x})w(\mathbf{x}+\mathbf{r}) \rangle, \quad (57)$$

where we disregard the corrections to Kolmogorov scaling that would become relevant at large Reynolds numbers. The self-consistency of the assumption of fast decay demands that $\langle w(\mathbf{x})w(\mathbf{x}+\mathbf{r}) \rangle$ decays with r faster than $r^{-4/3}$ - otherwise the pair-correlation function would not be a decaying function of the distance.

Formula (57) holds in all cases where the description with weakly compressible flow holds. If we use it in the case of inertial particles whose flow at small Stokes relaxation time τ (properly non-dimensionalized as small Stokes number) has $w = -\tau(\nabla_k u_i)(\nabla_i u_k)$ then the use of Kolmogorov scaling (dimensional analysis telling

that the only time-scale of turbulence relevant at scale r is t_r) gives $(\tau/t_r)^2$ for the RHS of Eq. (57) that is $\langle w(\mathbf{x})w(\mathbf{x}+\mathbf{r}) \rangle \propto r^{-8/3}$ and

$$\frac{\langle n(\mathbf{x})n(\mathbf{x}+\mathbf{r}) \rangle}{\langle n(\mathbf{x}) \rangle \langle n(\mathbf{x}+\mathbf{r}) \rangle} - 1 \sim \tau^2 \epsilon^{2/3} r^{-4/3}. \quad (58)$$

This scaling of the correlation function agrees with the prediction of the white noise model [5] however here the result is obtained without modelling the flow so it holds for Navier-Stokes turbulence.

In the case of diffusiophoretic particles at large Sc the range $l_d \ll r \ll \eta$ has no counterpart in the study of inertial particles. We have using Eq. (55) with $w = D_p \nabla^2 \ln C$,

$$\frac{\langle n(\mathbf{x})n(\mathbf{x}+\mathbf{r}) \rangle}{\langle n(\mathbf{x}) \rangle \langle n(\mathbf{x}+\mathbf{r}) \rangle} - 1 \approx D_p^2 \int_{-\infty}^0 \langle \nabla^2 \ln C[t_1, \mathbf{q}(t_1, \mathbf{x})] \nabla^2 \ln C[t_2, \mathbf{q}(t_2, \mathbf{x}+\mathbf{r})] \rangle dt_1 dt_2, \quad l_d \ll r \ll \eta. \quad (59)$$

We did not find a way for determining the r -dependence of the RHS. We can determine the order of magnitude using that at $r \sim l_0$ the correlation function has to agree with that at smaller scales given by Eq. (54),

$$\frac{\langle n(\mathbf{x})n(\mathbf{x}+\mathbf{r}) \rangle}{\langle n(\mathbf{x}) \rangle \langle n(\mathbf{x}+\mathbf{r}) \rangle} - 1 \sim \Delta, \quad r \sim l_0, \quad (60)$$

where the logarithmic factor in $t^* = |\lambda_3|^{-1} \ln(l_0/r)$ is of order one. The r -dependence of Eq. (59) could be determined using that the range of $l_d \ll r \ll \eta$ is characterized by one time-scale λ^{-1} so that the integration times in the integral are of order λ^{-1} giving,

$$\frac{\langle n(\mathbf{x})n(\mathbf{x}+\mathbf{r}) \rangle}{\langle n(\mathbf{x}) \rangle \langle n(\mathbf{x}+\mathbf{r}) \rangle} - 1 \sim \frac{D_p^2}{\lambda^2} \langle \nabla^2 \ln C(\mathbf{x}) \nabla^2 \ln C(\mathbf{x}+\mathbf{r}) \rangle, \quad l_d \ll r \ll \eta \quad (61)$$

Still, though the study of simultaneous correlation functions is simpler, we could not determine the r -dependence of the correlation function in the last line. This includes trying to perform the study in the simplest context solving the equations on the correlation functions of C obtained in the model where C is considered as passive field with no reaction on the flow and the statistics of the flow is modelled as decorrelated in time but correlated in space. It is this model of statistics that helped finding solutions for other correlation functions but in this case significant obstacles obstruct the solution [7]. However, we can use the obtained formula for experimental testing which will be done in Section VII.

VI. FLUCTUATIONS OF THE NUMBER OF PARTICLES IN GIVEN VOLUME

In this Section we provide detailed predictions for the statistics of particle distribution in space that include

the corrections due to discreteness of the number of particles. These corrections are relevant in situations where the number of particles in studied volumes is not too large which is often the case in experiments and numerical simulations. We use $t^* = |\lambda_3|^{-1} \ln(l'_0/l)$ where in the final formulas l_0 can be used instead of l'_0 , cf. the previous Sections.

Predictions for the statistics of concentration provided in the previous Sections were based on the continuity equation that neglects the discreteness of matter. It can be verified though that the derivation of the pair-correlation function can be performed directly for the particles using the identity for the particle's trajectory $\mathbf{x}(t)$,

$$\delta(\mathbf{x}(0) - \mathbf{x}) = \delta[\mathbf{x}(t) - \mathbf{x}(t, \mathbf{x})] \exp \left[- \int_t^0 w[t', \mathbf{x}(t', \mathbf{x})] dt' \right], \quad (62)$$

obtained from

$$\det[\nabla_k f_i(\mathbf{x})] \delta[\mathbf{f}(\mathbf{x})] = \delta(\mathbf{x} - \mathbf{x}_0), \quad \mathbf{f}(\mathbf{x}_0) = 0, \quad (63)$$

using $\mathbf{f}(\mathbf{x}) = \mathbf{x}(t, \mathbf{x}) - \mathbf{x}(t)$. This identity is the discrete counterpart of the solution (Eq. 33) of the continuity equation. We can then repeat the steps in the derivation of the pair-correlation function in the language of particles. For instance for the joint probability density function of positions of two particles,

$$P(\mathbf{x}_1, \mathbf{x}_2) = \langle \delta(\mathbf{x}_1(0) - \mathbf{x}_1) \delta(\mathbf{x}_2(0) - \mathbf{x}_2) \rangle, \quad (64)$$

we have

$$P(\mathbf{x}, \mathbf{x} + \mathbf{r}) = \langle \delta(\mathbf{x}_1(0) - \mathbf{x}) \delta(\mathbf{x}_2(0) - \mathbf{x} - \mathbf{r}) \rangle = \langle \delta(\mathbf{x}_1(-t^*) - \mathbf{x}(-t^*, \mathbf{x})) \delta(\mathbf{x}_2(-t^*) - \mathbf{x}(-t^*, \mathbf{x} + \mathbf{r})) \rangle \exp \left[- \int_t^0 dt' (w[t', \mathbf{x}(t', \mathbf{x})] + w[t', \mathbf{x}(t', \mathbf{x} + \mathbf{r}))] \right], \rangle$$

which is the counterpart of Eq. (34) for $t = -t^*$ that holds for the pair of trajectories $\mathbf{x}_1(t)$, $\mathbf{x}_2(t)$. Using the PDF of the particle position $P(\mathbf{x}) = \langle \delta(\mathbf{x}(0) - \mathbf{x}) \rangle$ we find

$$\frac{P(\mathbf{x}, \mathbf{x} + \mathbf{r})}{P(\mathbf{x})P(\mathbf{x} + \mathbf{r})} = \left(\frac{l_0}{r} \right)^{\Delta(\mathbf{x} + \mathbf{r}/2)}, \quad r \ll l_0. \quad (65)$$

Similar results hold for joint probability density function of N particles, see Eq. (46). However there are statistical properties where discreteness of matter demands different consideration. This is the case in Eq. (47) that gives

$$\frac{\langle N_l^k(\mathbf{x}) \rangle}{\langle N_l(\mathbf{x}) \rangle^k} = \left(\frac{l_0}{l} \right)^{\Delta(\mathbf{x})k(k-1)/2}, \quad (66)$$

that holds only provided that we can neglect that the number of particles N_l takes only integer values. This neglect is valid when the typical value of N_l is much larger

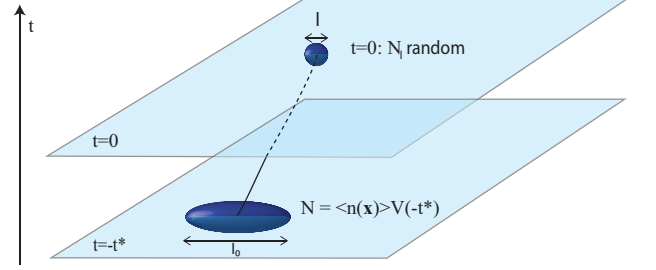


FIG. 2: Schematic illustrating how the randomness of the number of particles $N_l(0, \mathbf{x})$ becomes randomness of the growth factor of an infinitesimal volume in time t^* . The ball where the number of particles is studied is tracked back in time from $t = 0$ to the time $-t^*$ when it becomes an ellipsoid with largest size given by l'_0 . Since there are no concentration fluctuations over l'_0 the number of particles inside the ellipsoid's volume fluctuates as in an ideal gas (i.e. independent particles) with local average concentration. It is assumed that inhomogeneity of turbulent statistics occurs at larger scale so that the average concentration at the position of the volume at $t = -t^*$ equals the average concentration at the initial position $\langle n(\mathbf{x}) \rangle$ (thus $\ln(l_0/l)$ does not get too small which holds in practice).

than 1 which is often not the case in experiments (including numerical ones) demanding refinement. Fluctuations of $N_l(t, \mathbf{x})$ originate both from positive correlations of particles and discreteness of the number of particles (fluctuations of N_l when particles are uncorrelated are described by Poisson statistics), cf. [64].

We find statistics of the number of particles $N_l(\mathbf{x})$ within a ball of radius l centered at \mathbf{x} . We use the line of consideration of [19] illustrated in Fig. 2. Particles inside the ball at $t = 0$ were located at time $-t^*$ inside the ellipsoid whose largest size was l'_0 . Since over this scale the correlations of particles because of motion in the common flow are negligible [19] (the factor $f(\mathbf{x}, \mathbf{r}) \approx 1$ from $r \sim l'_0$) then the number of particles inside the ellipsoid obeys Poisson distribution with the average $\langle n(\mathbf{x}) \rangle$ times the volume of the ellipsoid. It is assumed here that inhomogeneity of turbulence occurs at scales larger than the size of the region covered by typical trajectories $\mathbf{x}(-t^*, \mathbf{x})$ so that the average concentration at the ellipsoid's position is $\langle n(\mathbf{x}) \rangle$.

Thus we consider the volume of the ellipsoid. The infinitesimal volume evolution obeys [65]

$$\frac{d \ln V}{dt} = \nabla \cdot \mathbf{v}[t, \mathbf{x}(t, \mathbf{x})], \quad V(0) = \frac{4\pi l^3}{3}, \quad (67)$$

$$V(t) = \frac{4\pi l^3}{3} \exp \left(- \int_t^0 \nabla \cdot \mathbf{v}[t', \mathbf{x}(t', \mathbf{x})] dt' \right). \quad (68)$$

This holds provided the volume size is smaller than l_0 . We comment on the case where the volume size is bigger than $l_0 = l_d$ when $l_d \ll \eta$. In this case when the volume size is larger than l_d but smaller than η the volume is still close to an ellipsoid. This is because the velocity difference of nearby particles is approximately given by that of the fluid particles which is distance times velocity gradient. However $\nabla \cdot \mathbf{v}$ varies over the volume so that Eq. (67) cannot be used.

In the continuum approximation the fluctuations of the number of particles in volume $V(-t^*)$ are neglected so that one sets $N_l(0, \mathbf{x})$ equal to the average number of particles $\langle n(\mathbf{x}) \rangle V(-t^*)$ inside $V(-t^*)$ deterministically. This gives Eq. (47).

Inclusion of discreteness of the number of particles gives that $N_l(0, \mathbf{x})$ at fixed $V(-t^*)$ is Poisson-distributed with the average $\langle n(\mathbf{x}) \rangle V(-t^*)$. Disregarding as previously the vicinity of time in the volume growth factor due to weak compressibility we conclude that we can perform independent averaging over $V(-t^*)$ and the number of particles inside $V(-t^*)$. We find using Poisson distribution for the number of particles in volume $V(t)$ with average concentration $\langle n(\mathbf{x}) \rangle$ that,

$$P[N_l(\mathbf{x}) = k] = \left\langle \frac{[\langle n(\mathbf{x}) \rangle V(-t^*)]^k \exp[-\langle n(\mathbf{x}) \rangle V(-t^*)]}{k!} \right\rangle_{V(-t^*)}, \quad (69)$$

where the remaining averaging is over the statistics of $V(-t^*)$. It is instructive that we consider low moments of $N_l(\mathbf{x})$. Since dispersion of the Poisson distribution is equal to the average then we have

$$\langle N_l^2(\mathbf{x}) \rangle = \langle n(\mathbf{x}) \rangle^2 \langle V^2(-t^*) \rangle + \langle n(\mathbf{x}) \rangle \langle V(-t^*) \rangle.$$

This averaging can be done simply observing that $V(-t^*)/(4\pi l^3/3)$ is the continuum variable $n_l(\mathbf{x})/\langle n(\mathbf{x}) \rangle$ obeying Eq. (47) so that,

$$\langle N_l^2(\mathbf{x}) \rangle = (4\pi l^3/3)^2 \langle n_l(\mathbf{x}) \rangle^2 + (4\pi l^3/3) \langle n(\mathbf{x}) \rangle. \quad (70)$$

Using Eq. (48) we find ($\langle N_l(\mathbf{x}) \rangle = (4\pi l^3/3) \langle n(\mathbf{x}) \rangle$)

$$\frac{\langle N_l^2(\mathbf{x}) \rangle}{\langle N_l(\mathbf{x}) \rangle^2} = \left(\frac{l_0}{l} \right)^{\Delta(\mathbf{x})} + \frac{1}{\langle N_l(\mathbf{x}) \rangle}, \quad l \ll l_0. \quad (71)$$

where the last term describes the correction to continuum approximation (66) due to discreteness. We observe that because the first term on the RHS is larger than one when the continuum approximation becomes valid in the limit where typically the volume contains large number of particles, $\langle N_l(\mathbf{x}) \rangle \gg 1$.

In contrast when $\langle N_l(\mathbf{x}) \rangle \ll 1$ we have large correction due to the discreteness that becomes relevant at scales $l \ll l_0$. This correction can be relevant in experiments and numerical simulations. The discreteness correction

to the third moment ($k = 3$ in Eq. (66)) is a power-law itself. We find using the third moment of Poisson distribution that

$$\langle N_l^3(\mathbf{x}) \rangle = \langle n(\mathbf{x}) \rangle^3 \langle V^3(-t^*) \rangle + 3 \langle n(\mathbf{x}) \rangle^2 \langle V^2(-t^*) \rangle + \langle N_l(\mathbf{x}) \rangle.$$

Thus using $\langle n(\mathbf{x}) \rangle V(-t^*) = \langle N_l(\mathbf{x}) \rangle n_l(\mathbf{x}) / \langle n(\mathbf{x}) \rangle$ we obtain,

$$\frac{\langle N_l^3(\mathbf{x}) \rangle}{\langle N_l(\mathbf{x}) \rangle^3} = \frac{\langle n_l^3(\mathbf{x}) \rangle}{\langle n_l(\mathbf{x}) \rangle^3} + \frac{3 \langle n_l^2(\mathbf{x}) \rangle}{\langle N_l(\mathbf{x}) \rangle \langle n_l(\mathbf{x}) \rangle^2} + \frac{1}{\langle N_l(\mathbf{x}) \rangle^2}. \quad (72)$$

We find using Eq. (48) that,

$$\frac{\langle N_l^3(\mathbf{x}) \rangle}{\langle N_l(\mathbf{x}) \rangle^3} = \left(\frac{l_0}{l} \right)^{3\Delta(\mathbf{x})} + \frac{3}{\langle N_l(\mathbf{x}) \rangle} \left(\frac{l_0}{l} \right)^{\Delta(\mathbf{x})} + \frac{1}{\langle N_l(\mathbf{x}) \rangle^2}.$$

If the average number of particles in the ball is small, $N_{l_0} \ll 1$, though the third-order scaling dominates the smallest scales, the discreteness produces a power-law correction that starts to dominate the scaling already at $l \ll l_0$. Thus due to the discreteness the third moment's dependence on the scale of coarse-graining at $l \ll \eta$ is a superposition of two power laws and not one power-law as is the case for the continuum.

The consideration for higher-order moments can be performed based on,

$$\exp[-\lambda] \sum_{k=0}^{\infty} \frac{k^n \lambda^k}{k!} = \sum_{k=1}^n \lambda^k S(n, k),$$

where $S(n, k)$ are Stirling numbers of the second kind [66]. We find

$$\langle N_l^n(\mathbf{x}) \rangle = \sum_{k=1}^n \langle N_l(\mathbf{x}) \rangle^k \frac{\langle n_l^k(\mathbf{x}) \rangle}{\langle n(\mathbf{x}) \rangle^k} S(n, k),$$

which gives ($S(n, n) = S(n, 1) = 1$),

$$\frac{\langle N_l^n(\mathbf{x}) \rangle}{\langle N_l(\mathbf{x}) \rangle^n} = \left(\frac{l_0}{l} \right)^{\Delta(\mathbf{x})n(n-1)/2} + \sum_{k=2}^{n-1} \frac{S(n, k)}{\langle N_l(\mathbf{x}) \rangle^{n-k}} \left(\frac{l_0}{l} \right)^{\Delta(\mathbf{x})k(k-1)/2} + \frac{1}{\langle N_l(\mathbf{x}) \rangle^{n-1}},$$

where the first line is obtained by neglecting discreteness of the number of particles and the second line describes the corrections due to discreteness vanishing in the limit of large $\langle N_l(\mathbf{x}) \rangle$. The considered cases of $n = 2, 3$ can be reproduced using the known values of $S(n, k)$.

Finally the study of moments of fractional order can be done using the probability density function of $N_l(\mathbf{x})$. We write Eq. (69) in the form

$$P[N_l(\mathbf{x}) = k] = \frac{\langle N_l(\mathbf{x}) \rangle^k}{k!} \left\langle \exp \left[-k \int_{-t^*}^0 \nabla \cdot \mathbf{v}[t, \mathbf{x}(t, \mathbf{x})] dt - \langle N_l(\mathbf{x}) \rangle \exp \left(- \int_{-t^*}^0 \nabla \cdot \mathbf{v}[t, \mathbf{x}(t, \mathbf{x})] dt \right) \right] \right\rangle. \quad (73)$$

This clearly obeys the normalization condition $\sum_{k=0}^{\infty} P[N_l(\mathbf{x}) = k] = 1$. We introduce a Gaussian variable,

$$\rho(\mathbf{x}) = \frac{1}{\ln(l'_0/l)} \ln \left(\frac{n_l(\mathbf{x})}{\langle n(\mathbf{x}) \rangle} \right) = \frac{1}{\ln(l'_0/l)} \int_{-t^*}^0 w[t, \mathbf{q}(t, \mathbf{x})] dt,$$

cf. Eq. (47) and Gaussian averaging of exponents in previous Sections (the integral is roughly the sum of large $\sim \lambda t^*$ independent random variables. Gaussianity can be proved using the cumulant expansion theorem [63]). The distribution is determined by the average and the dispersion,

$$\langle \rho(\mathbf{x}) \rangle = \frac{\Delta(\mathbf{x})}{2}, \quad \langle \rho^2 \rangle - \langle \rho \rangle^2 = \frac{\Delta(\mathbf{x})}{\ln(l'_0/l)}. \quad (74)$$

We find (we omit the spatial dependence of involved quantities)

$$P(N_l = k) = \frac{\langle N_l \rangle^k}{k!} \sqrt{\frac{\ln(l'_0/l)}{2\pi\Delta}} \int d\rho \exp \left[-\langle N_l \rangle \left(\frac{l}{l'_0} \right)^\rho + \ln \left(\frac{l}{l'_0} \right) \left(\frac{[\rho - \Delta/2]^2}{2\Delta} + k\rho \right) \right]. \quad (75)$$

We find using integration variable $\rho' = \rho + (k - 1/2)\Delta$ that

$$P[N_l = k] = \left(\frac{l'_0}{l} \right)^{\Delta k(k-1)/2} \frac{\langle N_l \rangle^k}{k!} \sqrt{\frac{\ln(l'_0/l)}{2\pi\Delta}} \int d\rho' \exp \left[-\langle N_l \rangle \left(\frac{l'_0}{l} \right)^{(k-1/2)\Delta} \left(\frac{l}{l'_0} \right)^{\rho'} - \ln \left(\frac{l'_0}{l} \right) \frac{\rho'^2}{2\Delta} \right],$$

where we used,

$$\frac{[\rho - \Delta/2]^2}{2\Delta} + k\rho = \frac{1}{2\Delta} (\rho + (k - 1/2)\Delta)^2 - \frac{k(k-1)\Delta}{2}.$$

The integral contains a large parameter so it is determined by ρ_* that gives maximum to the exponent. Taking the derivative of the exponent we find that this can be written in the form $\rho_* \ln(l'_0/l) = x$ where,

$$c \exp[-x] = x, \quad c = \langle N_l \rangle \left(\frac{l'_0}{l} \right)^{(k-1/2)\Delta} \ln \left(\frac{l'_0}{l} \right) \Delta. \quad (76)$$

We write the equation on x in the form $x = \ln c - \ln x$ which first iteration gives $x = \ln c - \ln(\ln c - \ln x)$. If $\langle N_l \rangle$ is not too small so that $\ln \ln c \ll \ln c$ then we find $x \approx \ln c - \ln(\ln c)$. We find using the maximum condition in the integrand,

$$P[N_l = k] \approx \left(\frac{l'_0}{l} \right)^{\Delta k(k-1)/2} \frac{\langle N_l \rangle^k}{k!} \sqrt{\frac{\ln(l'_0/l)}{2\pi\Delta}} \int d\rho' \exp \left[-\frac{(\rho' - \rho_*)^2}{2} \frac{\rho_* \ln^2(l'_0/l) - \ln(l'_0/l)}{\Delta} \right],$$

where the self-consistency of the assumption of strong peak at the maximum is $\ln(l'_0/l) \gg 1$. We find

$$P[N_l = k] \approx \left(\frac{l'_0}{l} \right)^{\Delta k(k-1)/2} \frac{\langle N_l \rangle^k}{k!} \frac{1}{\sqrt{x-1}} \exp \left(-\frac{1}{\ln(l'_0/l) \Delta} \left[x + \frac{x^2}{2} \right] \right). \quad (77)$$

This provides the closed form for the probability density function of the number of particles N_l . If k is not too small so that the Stirling formula for $k!$ can be used (which holds when $k \geq 10$ very well) then,

$$\ln P[N_l = k] \approx \ln \left(\frac{l'_0}{l} \right) \frac{\Delta k(k-1)}{2} + k \ln \langle N_l \rangle - k \ln k + k - \frac{\ln(2\pi k) + \ln(x-1)}{2} - \frac{1}{\ln(l'_0/l) \Delta} \left[x + \frac{x^2}{2} \right]. \quad (78)$$

We find using $x = \ln c - \ln(\ln c)$ that

$$x \approx \ln \left(\frac{l'_0}{l} \right) (k - 1/2) \Delta + \ln \langle N_l \rangle - \ln \left(k - \frac{1}{2} + \frac{\ln \langle N_l \rangle + \ln(\ln(l'_0/l) \Delta)}{\ln(l'_0/l) \Delta} \right), \quad (79)$$

which gives

$$\begin{aligned} \ln P[N_l = k] \approx & -\ln \left(\frac{l'_0}{l} \right) \frac{\Delta}{8} + \frac{\ln \langle N_l \rangle + 1}{2} \\ & - \frac{\ln(2\pi k) + \ln(x-1)}{2} - \frac{\ln \langle N_l \rangle}{\ln(l'_0/l) \Delta} + \frac{1}{\ln(l'_0/l) \Delta} \\ & \times \ln \left(k - \frac{1}{2} + \frac{\ln \langle N_l \rangle + \ln(\ln(l'_0/l) \Delta)}{\ln(l'_0/l) \Delta} \right) - \frac{\ln^2 \langle N_l \rangle}{2 \ln(l'_0/l) \Delta} \\ & - \frac{1}{2 \ln(l'_0/l) \Delta} \ln^2 \left(k - \frac{1}{2} + \frac{\ln \langle N_l \rangle + \ln(\ln(l'_0/l) \Delta)}{\ln(l'_0/l) \Delta} \right) \\ & + \frac{\ln \langle N_l \rangle}{\ln(l'_0/l) \Delta} \ln \left(k - \frac{1}{2} + \frac{\ln \langle N_l \rangle + \ln(\ln(l'_0/l) \Delta)}{\ln(l'_0/l) \Delta} \right) \\ & - \frac{1}{2} \ln \left(k - \frac{1}{2} + \frac{\ln \langle N_l \rangle + \ln(\ln(l'_0/l) \Delta)}{\ln(l'_0/l) \Delta} \right) \\ & + k \ln \left(1 - \frac{1}{2k} + \frac{\ln \langle N_l \rangle + \ln(\ln(l'_0/l) \Delta)}{k \ln(l'_0/l) \Delta} \right). \quad (80) \end{aligned}$$

This detailed formula describes the probability providing the Stirling formula can be used for $k!$. This works for $k > 7$ well so we kept $-1/2$ factor in $k - 1/2$. Further simplification is obtained in the limit of large k where in the last term the argument of the logarithm is close to one. Then we find log-normal distribution reproducing the continuum limit described in the previous Sections.

VII. EXPERIMENTAL CONFIRMATION OF PHORETIC CLUSTERING

According to the theory outlined above, phoresis leads to clustering of particles independent of the phoretic

mechanism. These predictions generally relate to scales smaller than the smoothness scale l_0 , but effects are also expected above this scale which is the range investigated experimentally. For the experimental analysis of phoretic clustering, we chose a turbulent flow with an inhomogeneous distribution of salinity in order to generate diffusiophoretic particle drift. This may also serve as a possible model for the formation of marine snow in the ocean. In the experiment, we examine the existence and the degree of particle clustering by measuring the pair correlation function of particle concentration and check the agreement with the theoretical predictions provided in the previous Sections.

An inclined gravity current setup is used to analyze the diffusiophoretic effect on particles in turbulent flow. The experimental setup is described in detail by [67]. The facility, shown schematically in Fig. 3, allows to create a turbulent flow that features strong local gradients of salinity. The current is realized as a turbulent flow of water, mixed with 1.8 vol% ethanol, rising along an inclined wall in a tank filled with dyed saltwater that is initially at rest. The small amount of ethanol in the light fluid serves to match the refractive indices of both fluids — a crucial prerequisite for optical flow measurements. For simplicity we will nevertheless refer to the mixture of water and ethanol as clear fluid in the following. An inhomogeneous salt distribution inside the turbulent fluid is created by entrainment of the saltwater into the lighter turbulent fluid from below. A snapshot of the resulting salt concentration field is shown in Fig. 4a.

Employing a recently developed measurement technique [68] that combines scanning 3D particle tracking velocimetry (3D PTV) and scanning laser induced fluorescent measurements (LIF) allows us to obtain both the 3D velocity and the concentration along Lagrangian particle trajectories. The volume of investigation measures $4 \times 2 \times 4 \text{ cm}^3$ in the streamwise (x), the spanwise (y) and the wall normal (z) direction, respectively. Using the method of Lüthi et al. [69] we are able to access the full Lagrangian velocity gradient tensor. We also measure the Laplacian of the salt concentration indirectly by using the total derivative along particle trajectories, i.e. using $dC/dt = D_s \nabla^2 C$. The spatial resolution of the velocity measurement is approximately 4η and the LIF resolution is $4l_d$ in the plane of the light sheet ($x - z$) and about $90l_d$ in the scanning (y) direction.

In order to characterize the flow field outside the limited spatial domain of the 3D measurements, simultaneous planar particle image velocimetry (PIV) [67] and LIF measurements were performed on a domain located in the $x - z$ plane and the spanwise center of the tank. The domain extends 6 cm in the wall-normal and streamwise direction respectively. This results in a pixel resolution of approximately 0.2η and an average inter-particle distance of 4.5η . One major advantage that this technique brings is the significantly longer recording time compared to the 3D measurements, where the scanning procedure

Properties of Flow and Particles		
Re	4800	[-]
Re_{λ_T}	70	[-]
λ_T	0.51	[cm]
η	0.03	[cm]
λ	11.1	[1/s]
l_d	10^{-3}	[cm]
μ	10^{-3}	[Pa · s]
D_S	1.99×10^{-9}	[m ² /s]
ρ_p	1016	[kg/m ³]
τ_p	10^{-4}	[s]
d_p	2×10^{-3}	[cm]
D_p	1.25×10^{-9}	[m ² /s]
Sc	500	[-]
St	10^{-3}	[-]

TABLE II: Properties of the flow, the fluid, the salt and the particles used in the experiment. Where λ_T is the Taylor microscale and Re_{λ_T} the Taylor Reynolds number, respectively. The dynamic viscosity of the working fluid is written as μ . The diffusivity of the salt is denoted as D_S . The important particle properties presented are the particle density ρ_p , the particle diameter d_p and the resulting diffusiophoretic constant D_p , calculated according to [50]. The particle Stokes number St is computed by the ratio of the particle response time τ_p to the Kolmogorov time scale λ^{-1} . The particle response time is defined as $\tau_p = \frac{2d_p^2 \rho_p}{9\mu}$.

limits the duration of the recording. This provides generally more statistics which is crucial for measuring the pair-correlation function of the particle concentration n . Therefore we used the planar PIV/LIF measurements for the analysis of the particle concentration n .

The particles seeded in the flow are injected before the inlet of the gravity current (see Fig. 3). The size of the particles used in the experiment is of $\mathcal{O}(l_d)$ and their ζ -potential is approximately -35 mV , which implies a diffusiophoretic constant of $D_p = 1.24 \times 10^{-9} \text{ m}^2/\text{s}$ in NaCl according to [50]. Thus in the presence of salinity gradients theory predicts that particles will acquire a drift velocity (see Table I), which - according to our theoretical prediction - is expected to eventually induce clustering of particles. Relevant flow and particle properties of the experiment are summarized in Table II. Furthermore the particle concentration n is a property of major importance to the following analysis. It is obtained experimentally by counting the number of particles in a circle of diameter of 2η , according to the definition of Eq. (49). This size of the circle is chosen in order to find a sufficient number of particles (> 1) inside the circle.

An instantaneous snapshot of the normalized salt concentration C is plotted in Fig. 4a where a value of 1 represents unmixed salty water and thus the maximum salt concentration. Snapshots of the norm of the corresponding instantaneous gradient of C and $\ln C$ are shown in Fig. 4b & c, respectively. Since diffusiophoresis is driven by $|\nabla \ln C|$, the ubiquitous filaments of large values of

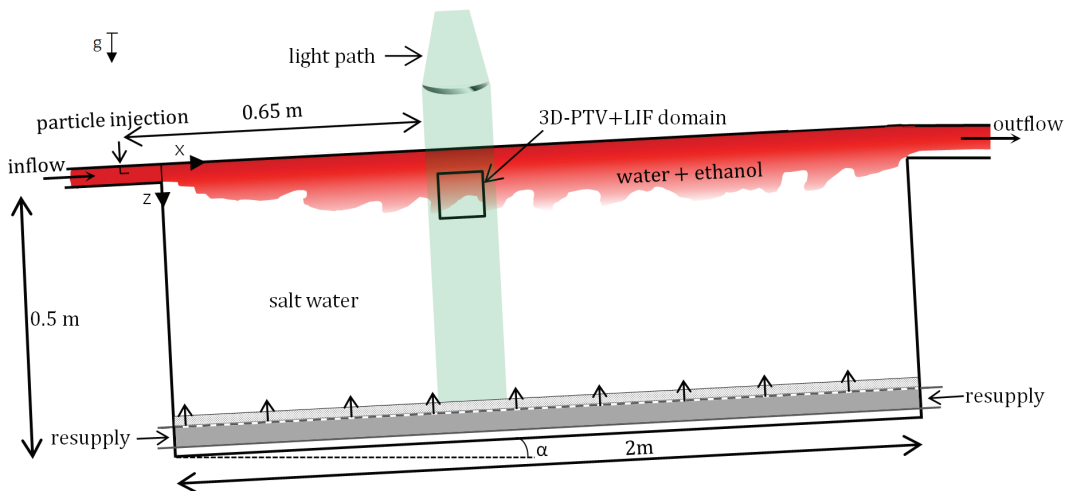


FIG. 3: Experimental setup showing the clear turbulent fluid (dark) rising along an inclined wall with angle ($\alpha = 10^\circ$). Entrained salt water (white) is gently resupplied through two perforated pipes on the bottom of the tank.

$|\nabla \ln C|$ (in Fig. 4c) indicate the regions where large difusiophoretic velocities are expected.

A. Profiles of average salt and particle concentration

The gravity current has one inhomogeneous direction, namely the wall-normal (z) direction, while y is the homogeneous and x the quasi-homogeneous coordinate (in particular, gradients of mean quantities are absent in y -direction and those in x -direction along the current have a characteristic length scale that is much larger than in z -direction). Profiles of particle and salt concentration averaged over the homogeneous directions are shown in Fig. 5a. Both, the average particle and the average salt concentration vary approximately linearly in depth over the so-called mixing layer ($\approx 40 \leq z/\eta \leq 100$). The average as well as the root-mean-square (rms) fluctuations of the salinity gradient shown in Fig. 5b are also strongly dependent on z , where the former is significantly smaller than the latter. Due to the significant variations of the salinity gradient in wall-normal direction we expect also the degree of clustering to vary in z -direction. For a detailed analysis we divided our measurement domain in 4 regions according to the wall-normal distance. The regions are indicated by the colored areas in Fig. 5, where dark colors represent lower salinity gradients and light colors high salinity gradients. We chose the regions such that $|\nabla C|$ is gradually increasing, as shown in Fig. 5. Bin I (dark) corresponds to almost clear fluid, whereas bin IV (bright) contains the highest salt concentration and salt concentration gradients.

B. Experimental Results

In this section we present the results of the experimental study on the pair-correlation function of the particle concentration. We obtain the pair-correlation of n from planar PIV/LIF measurements according to Eq. (49), where we substitute $(4\pi l^3)/3$ by πl^2 . The pair-correlation is evaluated in 4 regions and the results are presented in Figure 6. The pair correlation is plotted on a linear scale against the norm of the particle separation r in Fig. 6a and on a semi-logarithmic scale in Fig. 6b. The shaded patches in the upper plot indicate the experimental uncertainty of these measurements. This uncertainty is quantified by the standard deviation of the pair correlation function along the quasi-homogeneous streamwise direction. The pair correlation in region I stays almost constant at approximately 1 throughout all particle separations, indicating a homogeneous distribution of particles. However, the pair-correlation of region II, where significant concentration fluctuations are present, starts to deviate from 1 at scales $r \leq 8\eta$, showing minor inhomogeneities in the particle distribution at small separation scales. Further away from the top-wall, the data in regions III and IV display a higher level of salinity gradients (Fig. 5), which is accompanied by a stronger increase of the pair-correlation function at small particle separations in comparison to region II. The data points of region III and IV deviate from 1 at scales up to about 10 – 15 η (Fig. 6). The pair correlation in the regions II-IV is well approximated by a power law of the form $c_0(\eta/r)^{c_1(z)}$ (see Fig. 6b, where the fit parameters c_0 and c_1 are included in the legend). This power-law corresponds to the stretched exponential decay of the pair-correlation, cf. Eq. (58).

The exponent c_1 of the fit increases from 0 in region 1 to 0.04 in region 2 further to 0.072 in region 3 up to 0.08 in region 4. The pre-factor c_0 increases similarly

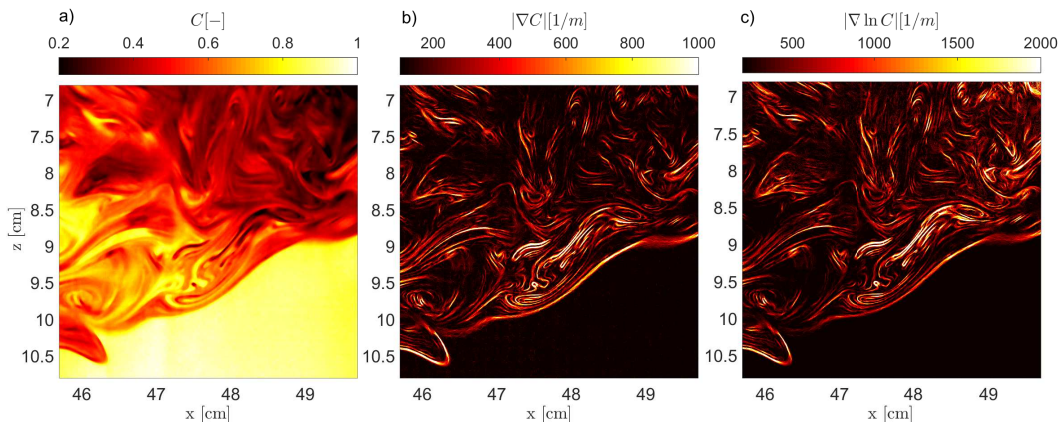


FIG. 4: Instantaneous snapshots in the central plane of the observation volume of salt concentration field with $C = 1$ being the maximum salt concentration (a), the corresponding norm of the gradient of the concentration field (b) and $|\nabla \ln C|$, which is the quantity that drives diffusiophoresis (c).

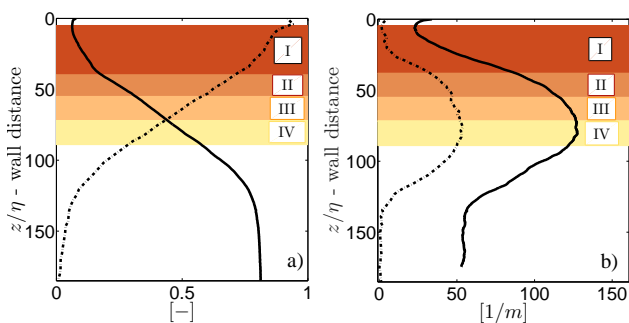


FIG. 5: Particle, salt concentration and salt concentration gradient averaged over time and homogeneous directions. a) Averaged particle concentration $n(z)$ (dashed-dotted line) and salt concentration $C(z)$ (continuous line) - b) averaged norm of the salinity gradient $|\nabla C(z)|$ (dashed-dotted line) and root-mean-square of the salinity gradient $(\nabla C)_{rms}$ (continuous line). The filled areas indicate 4 wall-parallel layers used for conditional averaging in section B below.

for higher bin numbers. The results show that the degree of particle clustering strongly depends on the inhomogeneous coordinate as predicted by the theory. The observed increase of clustering with larger wall distance seems plausible in view of the fact that the salty water mixes into the less dense and non-salty fluid from below, leading to high concentration gradients at some distance from the top wall. In order to validate these results and confirm that clustering is induced by diffusiophoresis, we estimate the clustering induced by the weak inertia of the particles. We use the second invariant of the velocity gradient tensor Q , to quantify the compressibility of the particle velocity that arises due to inertia. The 3D-PTV measurements are used to measure Q . From the second invariant of the velocity gradient tensor we obtain the Laplacian of pressure $\nabla^2 p$ along particle trajectories. The integral of the temporal correlation of $\nabla^2 p$ is a

measure for inertia induced clustering [19]. We obtain a scaling exponent Δ for inertial clustering on the order of 10^{-5} . Since Δ due to inertial clustering is several orders lower compared to the scaling exponents we get for the pair-correlation function ($c_1 = \mathcal{O}(10^{-2})$) in Fig. 6, we conclude that the observed clustering is not caused by inertia but by diffusiophoresis. Diffusiophoresis is driven directly by gradients of the logarithm of the concentration gradient and correspondingly stronger clustering in regions with stronger gradients is observed.

We compare the observed pair-correlation function with the theory. The theory does not describe the considered experimental situation exactly because in the present experiment there is no scale separation between the size of the particles and the smallest (Batchelor) scale of turbulence which is necessary so that the particle's velocity $\mathbf{v}(t)$ obeys $\mathbf{v} = \mathbf{u} + D_p \nabla \ln C$, see Table II. However the scales are of the same order of magnitude, thus the theory predicts that Eq. (59) holds by order of magnitude. We will further examine this in the following.

We use that Eq. (8) gives

$$\partial_t \ln C + \mathbf{u} \cdot \nabla \ln C = D_S \nabla^2 \ln C + D_S (\nabla \ln C)^2. \quad (81)$$

We make the assumption that both terms on the RHS of Eq. (81) have identical scaling in the correlation function so that the r -dependence of the pair-correlation function in Eq. (59) at $l_d \ll r \ll \eta$ can be obtained using,

$$\frac{\langle n(\mathbf{x})n(\mathbf{x} + \mathbf{r}) \rangle}{\langle n(\mathbf{x}) \rangle \langle n(\mathbf{x} + \mathbf{r}) \rangle} - 1 \propto D_p^2 \int_{-\infty}^0 \left\langle \left[\nabla^2 \ln C + (\nabla \ln C)^2 \right] [t_1, \mathbf{q}(t_1, \mathbf{x})] \left[\nabla^2 \ln C + (\nabla \ln C)^2 \right] [t_2, \mathbf{q}(t_2, \mathbf{x} + \mathbf{r})] \right\rangle dt_1 dt_2,$$

where proportionality designates that both sides have similar \mathbf{r} dependence. This assumption is highly plausible because the ratio of $\nabla^2 \ln C$ and $(\nabla \ln C)^2$ involves the slowly varying field $\ln C(\mathbf{x})$ that changes over the

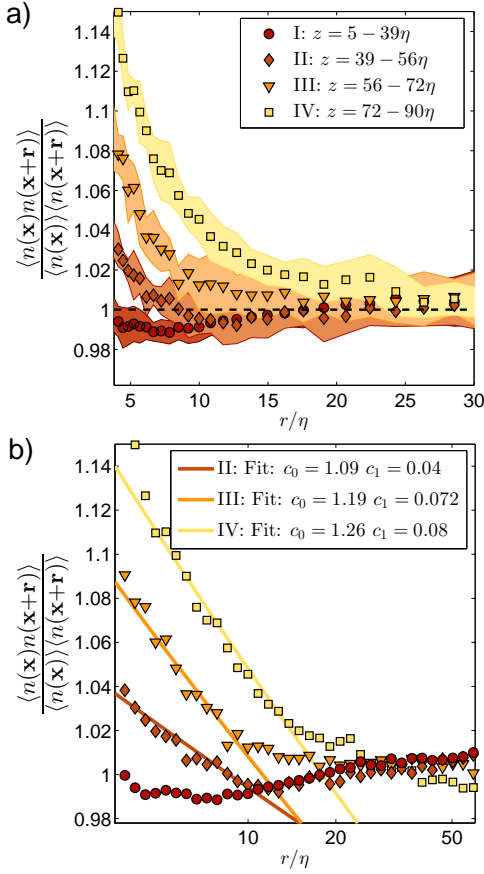


FIG. 6: Correlation of the particle concentration (Eq. 48), binned along z -direction in linear (a) and logarithmic (b) scale. The shaded patch in plot (a) indicates the standard deviation of this pair-correlation in streamwise direction. The colored lines indicate possible fits using $c_0 \left(\frac{\eta}{r}\right)^{c_1(z)}$ for the different bins. The magnitude of the salinity gradient is generally low in bins marked with darker color and gradually increasing while going to lighter colors.

scale η . Then using the material derivative along the fluid particle trajectory yields,

$$\frac{d}{dt} \ln C[t, \mathbf{q}(t, \mathbf{x})] = [\partial_t C + \mathbf{u} \cdot \nabla] \ln C, \quad (82)$$

with Eq. (81) we find,

$$\begin{aligned} \frac{\langle n(\mathbf{x})n(\mathbf{x}+\mathbf{r}) \rangle}{\langle n(\mathbf{x}) \rangle \langle n(\mathbf{x}+\mathbf{r}) \rangle} - 1 &\sim \frac{D_p^2}{D_S^2} \lim_{\Delta t \rightarrow \infty} \int_{-\Delta t}^0 dt_1 dt_2 \\ &\left\langle \frac{d}{dt_1} \ln C[t_1, \mathbf{q}(t_1, \mathbf{x})] \frac{d}{dt_2} \ln C[t_2, \mathbf{q}(t_2, \mathbf{x}+\mathbf{r})] \right\rangle \\ &= \frac{D_p^2}{D_S^2} \lim_{\Delta t \rightarrow \infty} \left\langle \ln \left(\frac{C(0)}{C(-\Delta t)} \right)_1 \ln \left(\frac{C(0)}{C(-\Delta t)} \right)_2 \right\rangle, \quad (83) \end{aligned}$$

where the indices 1 and 2 denote the two particles' trajectories that pass through the points \mathbf{x} and $\mathbf{x} + \mathbf{r}$ at $t = 0$. The correlation function in Eq. (83) is symmetric with respect to the change $\Delta t \rightarrow -\Delta t$ due to the incompressibility of turbulence.

We remark that the integral of the correlation function of time derivatives $d \ln C / dt$ vanishes when $r = 0$ because it becomes the integral of a complete time derivative. However this degeneracy disappears in the range $r \gtrsim \eta$ (as confirmed by experimental observations) so that the order of magnitude estimates above, hold.

It is this theoretical prediction (83) that we use for comparison with the experiment. This form does not involve the spatial differentiation of the concentration field that would increase the error significantly since $|\nabla C|$ varies over the smallest, (Batchelor) scale l_d , which is not fully resolved in our measurements.

To evaluate Eq. (83) experimentally, we considered the salt concentration along pairs of trajectories separated by a distance \mathbf{r} at a specific time t . This analysis requires the evaluation of 3D data. Therefore the results of the combined scanning 3D-PTV/LIF are used for the following results. We determined the salt concentration on the trajectories at times t and $t \pm \Delta t$, subsequently taking the average over all pairs of trajectories.

The correlation of Eq. (83) as a function of the particle separation \mathbf{r} is shown in Fig. 7. We did not study the dependence of $\langle n(\mathbf{x})n(\mathbf{x}+\mathbf{r}) \rangle$ on the direction of \mathbf{r} because of the strong anisotropy of the flow (difference between vertical and horizontal directions). This would demand a significantly larger pool of data and is beyond the scope of the present work. The different markers in Fig. 7 represent different Δt over which the salinity concentration has been tracked along pairs of trajectories. The curves shift upwards with increasing Δt and they gradually approach each other. The distance between the two curves at $\Delta t = 3\tau_\eta$ and $\Delta t = 3.5\tau_\eta$ is rather small. We obtained good convergence for the limit of infinite Δt over few Kolmogorov time-scales λ^{-1} , cf. Eq. (61) and Fig. 7 discussed below. However it is necessary to obtain a large number ($\geq 10^4$) of pairs of trajectories to achieve convergence because of the strong fluctuations of C , see the PDF of C in the inset of Fig. 7. The full convergence of Δt independent of the limit is expected to occur at about $5\tau_\eta$ [19] which is out of reach for the present experiment due to the limited length of trajectories.

The dashed line in Fig. 7 is a power law fit of the form $c_0(\eta/r)^{c_1}$ to the curve at $\Delta t = 3.5\tau_\eta$ with $c_1 = 0.012$ and a prefactor c_0 of 1.09. Comparing this with the direct measurements of the pair-correlation function (where we obtained values between 1 and 1.26 for c_0 and values ranging from 0 to 0.08 for c_1 depending on the z -position) we conclude that the experiment confirms the theoretical prediction (83).

Finally we compare the order of magnitude of the pair-correlation function with Δ which is predicted to give the order of magnitude of the pair correlation at the scale l_d , see Eq. (60). We have

$$\Delta = \frac{D_p^2}{|\lambda_3|} \int_{-\infty}^{\infty} \langle \nabla^2 \ln C(0) \nabla^2 \ln C(t) \rangle dt \sim \frac{D_p^2}{\lambda^2} \langle |\nabla^2 \ln C|^2 \rangle$$

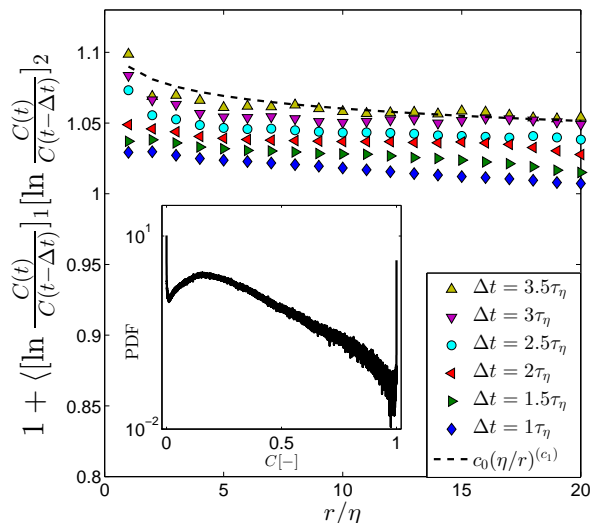


FIG. 7: Spatial correlation of $\ln C$ along pairs of trajectories plotted against the particle separation distance. Increasing Δt increases also the absolute value of the correlation. The power-law behavior of the data at $\Delta t = 3.5\tau_\eta$ is approximated by the dashed line, with the coefficients $c_0 = 1.09$ and $c_1 = 0.012$. Inset: PDF of C showing fluctuations over two orders of magnitude.

and we use this to approximate Δ by

$$\Delta \sim \frac{D_p^2}{\lambda^2 D_S^2} \left\langle \left| \frac{d \ln C}{dt} \right| \right\rangle^2. \quad (84)$$

We find $(D_p^2/\lambda^2 D_S^2) \langle |d(\ln C)/dt| \rangle^2$ to be 0.15 in our experiment. This provides reliably that Δ is approximately 0.15. Comparing this value with the measurements of the pair-correlation function we conclude that

$$\frac{\langle n(\mathbf{x})n(\mathbf{x} + \mathbf{r}) \rangle}{\langle n(\mathbf{x}) \rangle \langle n(\mathbf{x} + \mathbf{r}) \rangle} - 1 \sim \Delta, \quad r \sim \eta. \quad (85)$$

Comparison with Eq. (60) leads to the conclusion that the pair-correlation function does not decrease by order of magnitude in the Batchelor range $l_d < r < \eta$. This is quite reasonable since $\eta/l_d \sim 10$ is not too large.

VIII. DISCUSSION AND CONCLUSIONS

In this paper we demonstrated that phoretic particles that perform steady motion at a constant velocity $v_{ph} = c_{ph} \nabla \phi$ in the presence of gradients of the field ϕ in a fluid at rest, will move in the flow $\mathbf{u}(t, \mathbf{x})$ with the speed

$$\mathbf{v}(t) = \mathbf{u}[t, \mathbf{x}(t)] + c \nabla \phi[t, \mathbf{x}(t)], \quad (86)$$

provided that the characteristic temporal and spatial scales of the flow are above the characteristic scales of the phoretic phenomenon. The particles' motion in space

fits the frame of weakly compressible flow,

$$\frac{d\mathbf{x}}{dt} = \mathbf{v}[t, \mathbf{x}(t)], \quad |\nabla \cdot \mathbf{v}| \ll |\nabla \mathbf{v}|. \quad (87)$$

Thus we could use the theory of the distribution of particles in weakly compressible random flows [6, 19] for predicting that phoretic particles distribute in space over a multi-fractal set with the pair-correlation function of the particle concentration n obeying

$$\frac{\langle n(\mathbf{x})n(\mathbf{x} + \mathbf{r}) \rangle}{\langle n(\mathbf{x}) \rangle \langle n(\mathbf{x} + \mathbf{r}) \rangle} = \left(\frac{l_0}{r} \right)^{\Delta(\mathbf{x} + \mathbf{r}/2)}, \quad r \ll l_0, \quad (88)$$

where l_0 is the smallest of the Kolmogorov and Batchelor scales. The function $\Delta(\mathbf{x})$, given by Eq. (28), varies in space over the scales of inhomogeneity of the statistics of turbulence. The positivity of $\Delta(\mathbf{x})$ signifies divergence of the rms fluctuation of the concentration ($\langle n^2(\mathbf{x}) \rangle = \infty$) which manifests the distribution of particles over a singular multifractal set in space.

In the range $r \gtrsim l_0$ the correlations are weak, $\langle n(\mathbf{x})n(\mathbf{x} + \mathbf{r}) \rangle \approx \langle n(\mathbf{x}) \rangle \langle n(\mathbf{x} + \mathbf{r}) \rangle$. We determined the correction that corresponds to (where it can be proved) stretched exponential decay of $\langle n(\mathbf{x})n(\mathbf{x} + \mathbf{r}) \rangle / \langle n(\mathbf{x}) \rangle \langle n(\mathbf{x} + \mathbf{r}) \rangle$ to 1.

Equation (88) goes beyond the previous theory developed for spatially uniform statistics of turbulence [19]. It holds in the case of inhomogeneous turbulence provided the characteristic scale of inhomogeneity is not too small. Thus it can be used in a wide range of situations, including the experiment performed in this work.

Finally we derived statistics of the number of particles in a finite volume. This is necessary for dealing with discreteness of particles in experiments where the number of particles in volumes of interest is often not that large so that there are significant deviations from the continuum approximation. These predictions are useful for numerical simulations as well, helping to lower the capacity demanded for testing the theory. The derived statistics describe the changes, as compared to the Poissonian statistics of independent particles, due to correlations (i.e. power law corrections) induced by the motion of a finite number of particles monitored in a turbulent flow.

Our theoretical predictions apply to a wide range of phoretic phenomena. These include thermophoresis, diffusiophoresis, chemotaxis and electrophoresis. The prediction is based on the framework of weakly compressible flow that already proved itself in the study of interstitial particles and phytoplankton [40, 70]. However, the study of inhomogeneous turbulence and of the role of particles' discreteness which crucially extend the validity of the theory to many practical applications is the content of this work only.

Using simultaneous 3D particle tracking and concentration measurements in a turbulent gravity current, we confirmed the theoretical prediction of phoretic clustering in turbulent flow. We measured positive pair cor-

relations of diffusiophoretic particles that increase in regions of higher salinity gradients. Further, we confirmed these measurements using correlations of concentration over pairs of trajectories as well as order of magnitude estimates for gradients of concentration. Given that the particle size used in the experiment is of the same order as the Batchelor scale l_d , the experiments demonstrate clustering beyond the theoretical limits which increases the practical relevance and range of applications.

In the ocean l_d can well be of the order of the size of colloidal particles or smaller. The typical value for the energy dissipation ϵ per unit volume per unit time in

oceanic flows is $10^{-6}m^2/s^3$. Therefore the Kolmogorov time-scale is $\tau_\eta = \sqrt{\nu/\epsilon} \sim 1s$. Correspondingly $\eta = \nu^{3/4}\epsilon^{-1/4} = \tau_\eta^{3/2}\sqrt{\epsilon} \sim 10^{-3}m$, which gives $l_d \sim 10^{-5}m$. This length scale is comparable to typical sizes of colloidal particles in the ocean [71]. We thus conclude that diffusiophoresis may accelerate the agglomeration of organic matter and formation of marine snow.

Financial support from the Swiss National Science Foundation (SNSF) under Grant No. 144645 is gratefully acknowledged. We thank Thomas Kjørboe for helpful discussions.

-
- [1] U. Frisch, *Turbulence: the legacy of AN Kolmogorov* (Cambridge University Press, 1995).
- [2] H. Tennekes and J. L. Lumley, *A first course in turbulence* (MIT Press, 1972).
- [3] J. L. Anderson, *Annu. Rev. Fluid Mech.* **21**, 61 (1989).
- [4] M. Maxey, *J. Fluid. Mech.* **174**, 441 (1987).
- [5] E. Balkovsky, G. Falkovich, and A. Fouxon, *Phys. Rev. Lett.* **86**, 2790 (2001).
- [6] G. Falkovich, A. Fouxon, and M. Stepanov, *Nature* **419**, 151 (2002).
- [7] B. Devenish, P. Bartello, J.-L. Brenguier, L. Collins, W. Grabowski, R. IJzermans, S. Malinowski, M. Reeks, J. Vassilicos, L.-P. Wang, et al., *Q. J. Roy. Meteor. Soc.* **138**, 1401 (2012).
- [8] J. Bec, *Phys. Fluids* **15**, L81 (2003).
- [9] G. Falkovich and A. Pumir, *Phys. Fluids* **16**, L47 (2004).
- [10] J. Bec, K. Gawędzki, and P. Horvai, *Phys. Rev. Lett.* **92**, 224501 (2004).
- [11] J. P. Salazar, J. De Jong, L. Cao, S. H. Woodward, H. Meng, and L. R. Collins, *J. Fluid. Mech.* **600**, 245 (2008).
- [12] J. Bec, M. Cencini, and R. Hillerbrand, *Phys. Rev. E* **75**, 025301 (2007).
- [13] J. Bec, L. Biferale, M. Cencini, A. Lanotte, S. Musacchio, and F. Toschi, *Phys. Rev. Lett.* **98**, 084502 (2007).
- [14] E. Calzavarini, M. Cencini, D. Lohse, and F. Toschi, *Phys. Rev. Lett.* **101**, 084504 (2008).
- [15] P. Olla, *Phys. Rev. E* **81**, 016305 (2010).
- [16] M. Wilkinson, B. Mehlig, and K. Gustavsson, *Europhys. Lett.* **89**, 50002 (2010).
- [17] M. Wilkinson, B. Mehlig, and V. Bezuglyy, *Phys. Rev. Lett.* **97**, 048501 (2006).
- [18] R. A. Shaw, *Annu. Rev. Fluid Mech.* **35**, 183 (2003).
- [19] I. Fouxon, *Phys. Rev. Lett.* **108**, 134502 (2012).
- [20] G. Falkovich and A. Pumir, arXiv preprint nlin/0605040 (2006).
- [21] G. P. Bewley, E.-W. Saw, and E. Bodenschatz, *New J. of Phys.* **15**, 083051 (2013).
- [22] M. Wilkinson and B. Mehlig, *Europhys. Lett.* **71**, 186 (2005).
- [23] J. Bec, M. Cencini, and R. Hillerbrand, *Physica D* **226**, 11 (2007).
- [24] I. Fouxon and P. Horvai, *Phys. Rev. Lett.* **100**, 040601 (2008).
- [25] J. Bec, L. Biferale, G. Boffetta, A. Celani, M. Cencini, A. Lanotte, S. Musacchio, and F. Toschi, *J. Fluid Mech.* **550**, 349 (2006).
- [26] J. Jung, K. Yeo, and C. Lee, *Phys. Rev. E* **77**, 016307 (2008).
- [27] M. W. Vance, K. D. Squires, and O. Simonin, in *APS, Div. Fl. Dyn. 56th Annu. Meet. Abstracts* (2003), vol. 1.
- [28] A. Kaufmann, O. Simonin, and T. Poinsot, in *5th Int. Conf. on Multiph. Flow, Yokohama, Japan* (2004), p. 101.
- [29] P. Fevrier, O. Simonin, and K. D. Squires, *J. Fluid Mech.* **533**, 1 (2005).
- [30] M. W. Reeks, L. Fabbro, and A. Soldati, in *ASME 2006 2nd J. US-Eur. Fl. Eng. Sum. Meet.* (American Society of Mechanical Engineers, 2006), pp. 1755–1762.
- [31] K. Gustavsson, E. Meneguz, M. Reeks, and B. Mehlig, *New J. of Phys.* **14**, 115017 (2012).
- [32] S. Balachandar and J. K. Eaton, *Annu. Rev. Fluid Mech.* **42**, 111 (2010).
- [33] S. Elghobashi, W. Pun, and D. Spalding, *Numer. Pred. Flow, Heat Transf., Turb. and Combust* p. 188 (2013).
- [34] J. H. Seinfeld and S. N. Pandis, *Atmospheric chemistry and physics: from air pollution to climate change* (John Wiley & Sons, 2012).
- [35] R. C. Flagan and J. H. Seinfeld, *Fundamentals of air pollution engineering* (Courier Corporation, 2013).
- [36] A. Bracco, P. Chavanis, A. Provenzale, and E. Spiegel, *Phys. Fluids* **11**, 2280 (1999).
- [37] C. Crowe, M. Sommerfeld, and Y. Tsuji, Boca Raton, FL (1998).
- [38] W. A. Sirignano, *Fluid dynamics and transport of droplets and sprays* (Cambridge University Press, 1999).
- [39] I. Fouxon, Y. Park, R. Harduf, and C. Lee, *Phys. Rev. E* **92**, 033001 (2015).
- [40] W. M. Durham, E. Climent, M. Barry, F. De Lillo, G. Boffetta, M. Cencini, and R. Stocker, *Nat. Commun.* **4** (2013).
- [41] G. Károlyi, Á. Péntek, I. Scheuring, T. Tél, and Z. Toroczkai, *Proceedings of the National Academy of Sciences* **97**, 13661 (2000).
- [42] T. Nishikawa, Z. Toroczkai, C. Grebogi, and T. Tél, *Phys. Rev. E* **65**, 026216 (2002).
- [43] B. Abecassis, C. Cottin-Bizonne, C. Ybert, A. Ajdari, and L. Bocquet, *Nat. Mater.* **7**, 785 (2008).
- [44] J. Deseigne, C. Cottin-Bizonne, A. D. Stroock, L. Bocquet, and C. Ybert, *Soft matter* **10**, 4795 (2014).
- [45] R. Volk, C. Mauger, M. Bourgoïn, C. Cottin-Bizonne, C. Ybert, and F. Raynal, *Phys. Rev. E* **90**, 013027 (2014).

- [46] J. R. Taylor and R. Stocker, *Science* **338**, 675 (2012).
- [47] S. Belan, I. Fouxon, and G. Falkovich, *Phys. Rev. Lett.* **112**, 234502 (2014).
- [48] J. Wang and Z. Li, *Phys. Rev. E* **86**, 011201 (2012).
- [49] S. Hottovy, G. Volpe, and J. Wehr, *Europhys. Lett.* **99**, 60002 (2012).
- [50] J. L. Anderson and D. C. Prieve, *Separ. Purif. Method.* **13**, 67 (1984).
- [51] M. Smoluchowski and L. Graetz, *JA Barth, Leipzig* (1921).
- [52] E. F. Keller and L. A. Segel, *J. Theor. Biol.* **26**, 399 (1970).
- [53] R. Erban and H. G. Othmer, *SIAM J Appl. Math.* **65**, 361 (2004).
- [54] G. Batchelor, *J. Fluid. Mech.* **5**, 113 (1959).
- [55] H. Brenner, *Phys. Rev. E* **84**, 046309 (2011).
- [56] J. Kaplan and J. Yorke, in *Functional Differential Equations and Approximation of Fixed Points*, edited by H.-O. Peitgen and H.-O. Walther (Springer Berlin Heidelberg, 1979), vol. 730 of *Lecture Notes in Mathematics*, pp. 204–227.
- [57] G. Falkovich and A. Fouxon, *New. J. Phys.* **6**, 50 (2004).
- [58] P. Ditlevsen and I. Fouxon, *Manuscript in preparation* (2015).
- [59] V. I. Oseledets, *Trudy Moskovskogo Matematicheskogo Obshchestva* **19**, 179 (1968).
- [60] I. Goldhirsch, P.-L. Sulem, and S. A. Orszag, *Physica D* **27**, 311 (1987).
- [61] E. Balkovsky and A. Fouxon, *Phys. Rev.E* **60**, 4164 (1999).
- [62] G. Falkovich, K. Gawędzki, and M. Vergassola, *Rev. Mod. Phys.* **73**, 913 (2001).
- [63] S. Ma, *Statistical Mechanics* (World Scientific, 1985).
- [64] J. Bec, L. Biferale, M. Cencini, A. Lanotte, and F. Toschi, in *J Phys. Conf. Ser.* (IOP Publishing, 2011), vol. 333, p. 012003.
- [65] G. K. Batchelor, *An Introduction to Fluid Dynamics* (Cambridge University Press, 2000).
- [66] E. W. Weisstein, *CRC concise encyclopedia of mathematics* (CRC press, 2002).
- [67] D. Krug, M. Holzner, B. Lüthi, M. Wolf, W. Kinzelbach, and A. Tsinober, *Exp. Fluids* **54**, 1 (2013).
- [68] D. Krug, M. Holzner, B. Lüthi, M. Wolf, A. Tsinober, and W. Kinzelbach, *Meas. Sci. Technol.* **25**, 065301 (2014).
- [69] B. Lüthi, A. Tsinober, and W. Kinzelbach, *J. Fluid. Mech.* **528**, 87 (2005).
- [70] I. Fouxon and A. Leshansky, *Phys. Rev. E* **90**, 053002 (2014).
- [71] G. A. Jackson and A. B. Burd, *Environmental science & technology* **32**, 2805 (1998).